Variscan U-Th-Pb age for stratabound Pb-Zn mineralization in the Bossòst dome (Pyrenean Axial Zone)

Alexandre Cugerone, Françoise Roger, Bénédicte Cenki-Tok, Emilien Oliot, Jean-Louis Paquette

Ore Geology Reviews xxx (xxxx) 104503

Contents lists available at ScienceDirect

Ore Geology Reviews

journal homepage: www.elsevier.com/locate/oregeorev

Variscan U-Th-Pb age for stratabound Pb-Zn mineralization in the Bossòst dome (Pyrenean Axial Zone)

Alexandre Cugerone [a,*], Françoise Roger [a], Bénédicte Cenki [a], Emilien Oliot [a], Jean-Louis Paquette [b]

[a] Géosciences Montpellier, University of Montpellier, CNRS, Montpellier, France
[b] Laboratoire Magmas et Volcans, Campus Universitaire des Cézeaux, Aubière, France

ARTICLE INFO

Keywords:
Pb-Zn mineralization
Monazite
Zircon
LA-ICPMS U-Th-Pb geochronology
Pyrenees
Variscan orogeny

ABSTRACT

In orogens, pinpointing the timing of mineralization is often complex due to superimposition of magmatic, metamorphic and tectonic events. Unravelling the tectono-metamorphic evolution of deformed terranes is essential for understanding the formation of orogenic mineralization. In the Bossòst dome of the Pyrenean Axial Zone, undated stratabound Pb-Zn mineralization previously considered to be SEDEX-like and devoid of evidence for significant remobilization/deformation, was recently interpreted as orogenic mineralization and structurally-controlled by Variscan tectonics. However, relations with the poly-magmatic and metamorphic events reported in the Pyrenean Axial Zone are still poorly constrained. In the Bossòst dome, laser-ablation inductively coupled plasma mass spectrometry (LA-ICPMS) U-Th-Pb dating was performed on zircon to constrain the formation ages of two undeformed granitic dykes, and on monazite to identify both the metamorphic imprint recorded by two metapelites and the formation of stratabound Pb-Zn mineralization in the Bentaillou deposit. Late-Carboniferous – early-Permian magmatic zircon ages (315–280 Ma) are commonly found in these undeformed dykes (307.4 ± 4.7 Ma and 283 ± 15 Ma), consistent with the main magmatic event, extensively recorded in the Pyrenean Axial Zone. Monazite crystals with co-genetic textural relationships with stratabound sphalerite from Bentaillou were dated at 309 ± 11 Ma. We propose that the stratabound mineralization is formed during one main Variscan remobilization event associated with the first Variscan deformation event (D1) and probable metamorphic fluid circulation in pre-existing metal-rich Ordovician sedimentary levels. Moreover, monazite ages in metapelite rocks (289.1 ± 5.9 Ma and 290.0 ± 3.8 Ma) probably date both the end of high T-low P metamorphism and late fluid circulation in the Variscan tectonothermal event. Visean-Serpukhovian ages (340–325 Ma) are found in one inherited zircon and in two monazites included in garnet and staurolite, which probably record the end of the first Variscan magmatic-metamorphic event, mainly recorded in the core of the Pyrenean Axial Zone. Based on our ages and a regional synthesis, we propose a new tectono-metamorphic model for the Bossòst dome and the related formation of Pb-Zn mineralization.

1. Introduction

Determining the relative and absolute timing of ore formation in orogens with regards to granitic intrusion and metamorphism is generally challenging due to the superimposition of tectono-metamorphic events. Structures, ore textures and mineral emplacement may be difficult to interpret due to partial or total resetting and/or recrystallization of ore mineralization. In various orogenic Pb-Zn districts, the timing of mineralization and remobilization stages are debated and difficult to reconcile with geodynamic settings as, for example, in Australian sediment-hosted Pb-Zn deposits (Cave et al., 2020; Gibson et al., 2017; Gigon et al., 2020; Murphy, 2004; Perkins and Bell, 1998; Spinks et al., 2021) or in other base metal massive sulfide deposits (e.g. Admou et al., 2018; Chauvet et al., 2004; Essaifi et al., 2019; Marignac et al., 2003; Tornos et al., 2008). Therefore, regional investigations at multiple scale and involving ores and host-rocks are necessary to better constrain the timing of mineralization formation and possible late reworking.

Dating the emplacement of magmatic bodies is one of the most important indirect chronological approaches to constrain the emplacement of metamorphic and structurally-controlled ore mineralization as well as reaching a conclusion on the regional geodynamic evolution (e.g. Burisch et al., 2019; Jiang et al., 2020; Laurent et al., 2017;

* Corresponding author.
E-mail addresses: alex.cugerone@gmail.com (A. Cugerone), francoise.roger@umontpellier.fr (F. Roger), benedicte.cenki-tok@umontpellier.fr (B. Cenki), emilien.oliot@umontpellier.fr (E. Oliot), j.l.paquette@opgc.univ-bpclermont.fr (J.-L. Paquette).

https://doi.org/10.1016/j.oregeorev.2021.104503
Received 29 June 2021; Received in revised form 19 September 2021; Accepted 27 September 2021
0169-1368/

Martinez Catalan, 2011; Vanderhaeghe et al., 2020; Walter et al., 2018; Wu et al., 2018). In the Pyrenean Axial Zone (PAZ), a late-Carboniferous – early-Permian widespread magmatism (315–280 Ma) is well-documented (e.g. Carreras and Druguet, 2014; Denèle et al., 2014) but the existence of early-Carboniferous magmatism (Visean-Serpukhovian; 340–325 Ma) has been recently reported in the Bossòst, Aston (Soulcem granite) and Lys-Caillaouas metamorphic cores in the central part of the PAZ (Fig. 1) (Lopez-Sanchez et al., 2019; Mezger and Gerdes, 2016; Schnapperelle et al., 2020). The existence and origins of these two magmatic events are still rarely incorporated in recent geodynamic models of the PAZ (Denèle et al., 2014; Le Bayon and Cochelin, 2020) even if a few authors have proposed syn- and late-orogenic granite emplacement in their model (García-Sansegundo et al., 2011).

In the Pyrenees, Pb-Zn mineralization is widespread and were essentially mined during the 20th century (~400,000 t Zn and ~180,000 t Pb extracted). Stratabound (e.g. Pierrefitte, Bentaillou and Arditurri districts) and vein mineralization (e.g. Arre-Anglas district) are the two main documented mineralization events (Fig. 1B) (Bois et al., 1976; Castroviejo Bolibar and Serrano, 1983; Cugerone et al., 2018b; Cugerone et al., 2018a; Munoz et al., 2016; Nicol et al., 1997; Reyx, 1973). The largest known Pb-Zn ore bodies occur in stratabound veins hosted in metasedimentary rocks (clastic or carbonate-marble rocks). This mineralization-type has been interpreted as SEDEX and synchronous to Cambro-Ordovician, Devonian or Carboniferous (Bashkirian-Moscovian) sedimentations (Bois et al., 1976; Pesquera and Velasco, 1989; Pouit, 1986; Pouit, 1978) even if some authors questioned the Variscan overprints on mineralization genesis/remobilization in some localities (Alonso, 1979; Nicol et al., 1997). Based on various crustal Pb evolution models (e.g. Cumming and Richards, 1975; Stacey and Kramers, 1975), the lead isotope composition studies of Pyrenean galena generally indicate one metal source, and suggest a syngenetic emplacement age during Ordovician-Devonian extension periods for Pb-Zn stratabound mineralization in the Pyrenees, (Cardellach et al., 1996; García-Sansegundo et al., 2014; Marcoux, 1986; Marcoux et al., 1991; Velasco et al., 1996). Recent field and mineralogical study proposed that stratabound Pb-Zn mineralization formation is epigenetic, mainly controlled by Variscan D1 deformation and crosscuts by minor disseminated and stratiform Pb-Zn mineralization with probable syngenetic origin (Cugerone et al., 2018b). However, the age, the source, and the impact of Variscan deformation on stratabound Pb-Zn mineralization are still poorly constrained.

In the metamorphic core of the Bossòst dome (also known as Garona dome), we have performed LA-ICPMS U-Th-Pb dating on zircon and monazite from granitic dykes and metapelites in order to decipher the geochronological framework of the tectono-magmatic and metamorphic events of the PAZ. Moreover, in low-grade metamorphic rocks of the Bossòst dome, we have dated monazite genetically associated with sphalerite from the Bentaillou stratabound Pb-Zn mineralization in order to establish the ore formation age and its relationship with the Variscan tectono-metamorphic events.

2. Geological setting

2.1. Overview of the Pyrenean Axial Zone (PAZ)

2.1.1. Structural setting

The PAZ is the Paleozoic basement of the Pyrenees exhumed during the Pyrenean-Alpine tertiary orogeny and is bounded by the North and South Pyrenean zones where Mesozoic and Tertiary sedimentary rocks predominate (Fig. 1A) (Choukroune, 1992; Zwart, 1963a). The main tectono-metamorphic event recorded in the PAZ is Variscan in age (340–290 Ma) and is attributed to the convergence and subsequent subduction-collision of the Gondwana continent beneath Armorica micro-continents during the Upper Paleozoic (Matte, 2001; Stampfli et al.,

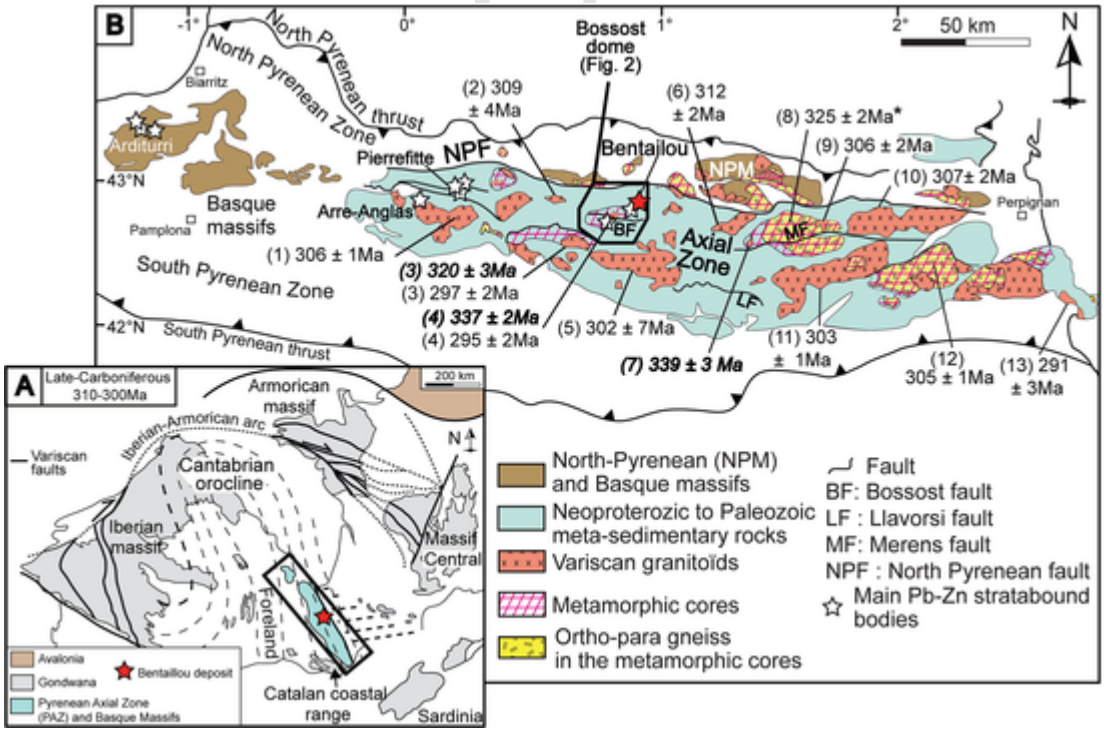

Fig. 1. A. Location of the PAZ and other domes in the Variscan belt of the Western Europe during late-Carboniferous. B: Simplified geological map of the Pyrenean Axial Zone (PAZ) with location of the basement and metamorphic domes. Some representative U-Th-Pb data are given in bold font for Visean granite, normal font for late-Carboniferous granite and with "*" for one metamorphic data. References: 1-Cauteret (Denèle et al., 2014); 2-Bordères-Louron (Gleizes et al., 2006); 3-Lys-Caillaouas (Lopez-Sanchez et al., 2019); 4-Bossòst (Lopez-Sanchez et al., 2019; Mezger and Gerdes, 2016); 5-Maladeta (Martínez et al., 2016); 6-Bassiès (Paquette et al., 1997); 7-Soulcem (Mezger and Gerdes, 2016); 8-Aston (Mezger and Gerdes, 2016); 9-Ax-les-Thermes (Denèle et al., 2014); 10-Quérigut (Roberts et al., 2000); 11-Mont-Louis (Denèle et al., 2014); 12-Canigou (Denèle et al., 2014); 13-Cap de Creus (Druguet et al., 2014).

2013). Nonetheless, there are some indications of Alpine deformation, generally restricted to regional south-directed thrusts in the PAZ (e.g. Carreras and Druguet, 2014; Cochelin et al., 2017b; Vergés et al., 2002). The PAZ is composed of Neoproterozoic to Paleozoic metasedimentary rocks and has been intruded by Ordovician or Carboniferous granitoids. High-grade metamorphic rocks are often reported in cores of gneiss domes, with orthogneisses derived from Ordovician granitoids (e.g. Cocherie et al., 2005; Deloule et al., 2002; Laumonier et al., 2004) (Fig. 1B).

The Variscan crust of the PAZ is usually subdivided into two main structural levels (e.g. De Sitter and Zwart, 1960; Kleinsmiede, 1960; Zwart, 1979): (i) the lower-crustal level named the Infrastructure, which is generally composed of high-grade metamorphic metasedimentary rocks and Ordovician orthogneiss (mainly in the eastern part of the PAZ), characterized by flat-lying foliation and a long-lived regional MT/MP Barrovian metamorphism (M1). Highly-deformed domains locally display steep and penetrative crenulation to penetrative foliations. Several peraluminous granitoids, such as the Ax-les-Thermes granite (emplacement age of 306.0 ± 2.3 Ma; Denèle et al., 2014), are locally reported in high-grade metamorphic areas and certainly originate from the partial melting of the Infrastructure (e.g. Denèle et al., 2014; Kilzi et al., 2016; Roberts et al., 2000). These anatectic granites generally record a high-temperature solid-state deformation imprint and HT-LP Buchan metamorphism is superimposed in surrounding rocks on the Barrovian (MT-MP) metamorphism. (ii) The upper-crustal level named the Suprastructure is generally weakly metamorphosed and characterized by steep fabrics with the presence of steep slaty cleavage in particular (Carreras and Capella, 1994; Carreras and Druguet, 2014; De Sitter and Zwart, 1960; Zwart, 1979). Most magmatic bodies in the PAZ are calc-alkaline granites (310–298 Ma; Denèle et al., 2014) and possible product of crustal magma-mixing (Debon, 1980; Gleizes et al., 2006; Lemirre et al., 2019; Vilà et al., 2005). They usually exhibit a poor solid-state deformation imprint (e.g. Denèle et al., 2014 and references therein) and small contact aureoles are often noticed close to these plutons in this structural level (Debon, 1980; Evans et al., 1998).

2.1.2. Tectono-metamorphic evolution

The chronology of tectonic and metamorphic events in the PAZ is debated and various geodynamic models have been proposed in the recent decades that incorporate the presence of doming structures, thought to have developed during extensional or transpressive deformation (Carreras and Capella, 1994; Denèle et al., 2014; García-Sansegundo et al., 2011; Laumonier et al., 2010; Martinez Catalan, 2011; Matte, 2001; Mezger and Gerdes, 2016; Mezger and Passchier, 2003; Pouget, 1991; Soula et al., 1986; Soula, 1982; Van den Eeckhout and Zwart, 1988). Nonetheless, recent structural studies focusing on the structural relationships between granites and metasedimentary rocks have led to models where intrusion emplacement during late-Carboniferous was coeval with crustal flow, dextral transpression and doming in an overall dextral strike-slip setting (Cochelin et al., 2017b; Denèle et al., 2014).

In the model proposed by Denèle et al. (2014) (modified after Laumonier et al., 2010), the deformation history can be described by three major stages: (i) an early-Variscan E-W deformation (D1) stage between 323–308 Ma related to crustal thickening and responsible for the formation of a flat-lying S1 foliation in the Infrastructure and a flat-to-steep S1 foliation in the Suprastructure. This D1 stage is synchronous to the regional M1 metamorphism with MT/MP staurolite-garnet assemblages (0.5 GPa and 580 °C; de Hoÿm de Marien et al., 2019; Mezger and Gerdes, 2016) (ii) A late-Variscan deformation stage (D2) between 308–300 Ma corresponding to the beginning of a Variscan magmatic event associated with doming and the end of thickening D1 phase. D2 deformation is composed of two main deformation stages. The D2a stage corresponds to horizontal and lateral crustal-flow mainly recorded in the Aston and Hospitalet orthogneiss of the Infrastructure (Denèle et al., 2014; Zwart, 1979) synchronous to magmatism and HT/LP peak of metamorphism observed close to Variscan plutons and cordierite superimposed assemblages (575–600 °C and 0.3 GPa; Mezger and Régnier, 2016). Moreover, a HT metamorphism at the contact with Variscan plutons is also reported with a few kilometric-scale metamorphic aureole in the upper crustal levels (Debon, 1980; Denèle et al., 2014). The D2b stage is related to the formation of metamorphic domes at 304 Ma and tight F2 folds with associated S2 cleavage, predominantly in the upper crust (Denèle et al., 2014). (iii) A younger late-Variscan transpressive stage (D3; 300–290 Ma) is characterized by metric-size E-W dextral shear-zones along regional faults, such as the Bossòst (Mezger, 2005) or the Merens faults (Carreras et al., 1980; Carreras and Cirés, 1986; Denèle et al., 2008; Mezger et al., 2012; Ostkamp et al., 2019; Van den Eeckhout, 1986). Nonetheless, this geodynamic model proposed by Denèle et al. (2014) does not incorporate recent Visean magmatic ages observed in the core of several metamorphic dome in the Pyrenees (Mezger and Gerdes, 2016). Another geodynamic model proposed by García-Sansegundo et al. (2011) reports polyphase magmatism with the presence of syn-orogenic granite formed between D1 and D2 deformation events and late-orogenic granite post-D2 event. Moreover, in this model, D2 deformation is highly controlled by numerous south-directed Variscan thrusts mainly in the regional Silurian black-schist levels.

2.1.3. Occurrence of a Visean-Serpukhovian event

The occurrence of Visean magmatism (340–325 Ma) in the PAZ was first described by Mezger and Gerdes (2016) and is still debated (Denèle et al., 2014; Lopez-Sanchez et al., 2019; Mezger and Gerdes, 2016; Schnapperelle et al., 2020). The onset of Variscan deformation is commonly considered as Serpukhovian- Baskirian in age (325–315 Ma) by Denèle et al. (2014), and is recorded by the *syn*-orogenic Carboniferous deposition of flysch in the low-grade metamorphic domains, regionally named the Culm facies (Delvolvé et al., 1993). However, a recent study based on regional paleobotanical data and textural observations on Carboniferous Culm rocks, east of the PAZ, has proposed a time span of Culm sedimentation between 330 and 319 Ma with two Variscan ductile deformations pre- and syn-Culm flysch deposition (Martín-Closas et al., 2018). The age of the pre-Visean deformation and the presence of undeformed igneous rocks in the Culm conglomerates is difficult to link to the model of Denèle et al. (2014), where the beginning of magmatism and deformation is considered Namurian in age (325 Ma). Moreover, in the central part of the PAZ (Aran Valley), detrital zircons of igneous origin have been reported from Culm flysch rocks and dated at 338 ± 2 Ma (Martínez et al., 2016).

The poorly deformed Late-Variscan granitoids are interpreted as contemporaneous to the dextral transpressive tectonic regime (312–300 Ma; e.g. Guitard et al., 1984; Paquette et al., 1997; Evans et al., 1998; Roberts et al., 2000; Carreras et al., 2004; Gleizes et al., 2006; Denèle et al., 2014) (Fig. 1B). Nevertheless, the Visean-Serpukhovian ages (340–325 Ma) obtained for the emplacement of the Bossòst and Soulcem granitoids in the deep crust, the migmatization of the Aston dome as well as the occurrence of Serpukhovian inherited zircon (331–323 Ma) from the Bossòst and Lys-Caillaouas leucocratic granitoids facies clearly demonstrate the occurrence of a proto-dome and restricted magmatism, Visean in age (Lopez-Sanchez et al., 2019; Mezger and Gerdes, 2016; Schnapperelle et al., 2020).

2.1.4. Stratabound Pb-Zn mineralization

In this tectonic-metamorphic framework, the chronology of stratabound Pb-Zn mineralization is still unclear. Mostly located in the central and western part of the PAZ, stratabound mineralization is hosted in clastic and carbonate rocks from Cambro-Ordovician to Devonian ages (Cugerone et al., 2018b; Pouit, 1985). This mineralization-type is mostly parallel to S0-S1 foliation or hosted in D1 thrusts and appears locally subsequently remobilized in F2 fold hinges or D2 thrusts

(Fig. 2B) (García-Sansegundo et al., 2014). Lead-zinc mineralization can be hosted in high-grade metamorphic rocks located in the Infrastructure as in the Victoria district, or in the low-grade metamorphic rocks of the Suprastructure as in the Pierrefitte or Bentaillou deposits (Fig. 2A-B). Based essentially on macrostructural concordance between mineralization and stratification, ore formation has been interpreted in many studies as Ordovician or Devonian in age and as the result of syngenetic processes with only minor local remobilization during the later

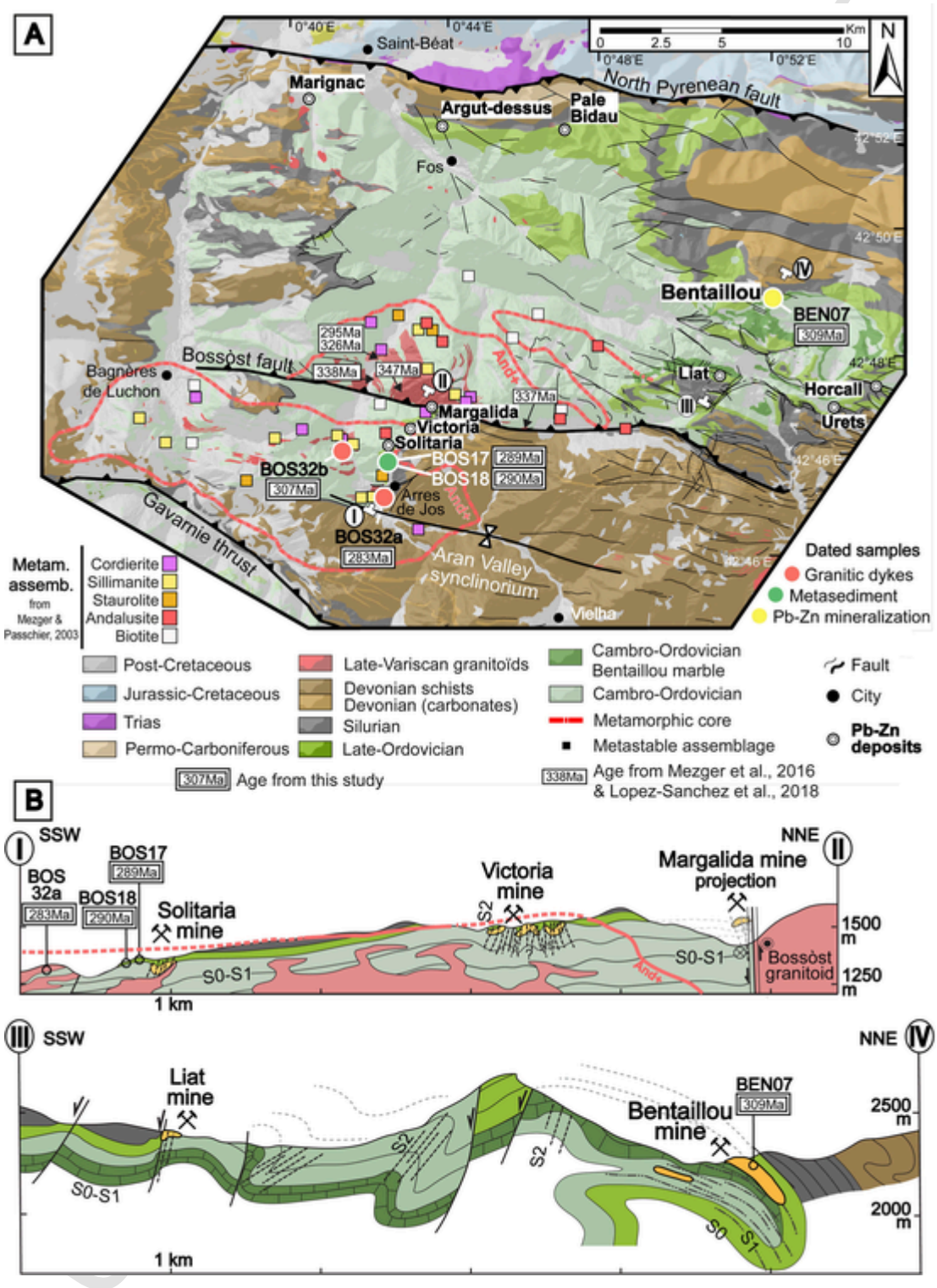

Fig. 2. A. Geological map of the Bossòst dome with samples locations and their corresponding ages (additionnal ages in the northern part of the Bossòst metamorphic core from Lopez-Sanchez et al., 2019; Mezger and Gerdes, 2016): two granitic dykes represented with red circles, two metasedimentary rocks represented with pink circles, and Bentaillou Pb-Zn mineralization at the east of the Bossòst dome represented with orange circles. Location of metamorphic mineral assemblages from Mezger and Passchier (2003) is indicated by colored squares. Abbreviations: NPF: North Pyrenean Fault; BF: Bossòst fault; GT: Gavarnie thrust. B. Two cross-sections of the southern and eastern part of the Bossòst dome. Location of the Bentaillou and other Pb-Zn mines are represented as well as position of the samples in the area (except BOS32b) (modified from Cugerone et al., 2018a; Cugerone et al., 2018b; García-Sansegundo and Alonso, 1989). (For interpretation of the references to colour in this figure legend, the reader is referred to the web version of this article.)

Variscan D2 tectonic event, and with no significant involvement of Variscan D1 tectonics (Cardellach et al., 1996; García-Sansegundo et al., 2014; Pouit, 1978; Pouit and Bois, 1986). Nonetheless, a recent regional field study of stratabound and vein Pb-Zn mineralizations in the PAZ indicated a syn-D1 mineralization, related to the opening of pull-apart type structures parallel to S1 foliation and transposed on S0 stratification, and in close association with D1 thrust or F1 kilometric-size recumbent folds. This new metallogenic model is also based on cross-cutting and kinematic indicators between sphalerite and metamorphic mineral (gahnite, garnet) and also demonstrates subsequent local remobilization of D2 tectonic (Cugerone et al., 2018b).

2.2. The Bossòst dome

2.2.1. Structures

The Bossòst dome is located in the central part of the PAZ, between the North Pyrenean Fault and the Aran Valley synclinorium (Figs. 1 and 2), and is composed of Cambro-Devonian metasedimentary rocks and a Variscan granitic complex associated with a metamorphic core, truncated by the E-W trending Bossòst fault (Cochelin, 2016; García-Sansegundo, 1996; Mezger and Passchier, 2003; Pouget, 1991). This fault is probably related to Variscan and/or Pyrenean-Alpine tectonics (Mezger, 2005). Structurally, Variscan D1 deformation is largely associated with the development of the generally E-W trending S1 foliation, into which S0 is frequently transposed. In the metamorphic core of the Bossòst dome, S1 is easily observed with aligment of metamorphic minerals (e.g. biotite, garnet, gahnite) or elongated quartz, and is clearly axial planar to large kilometric-size recumbent F1 folds in the two structural levels (García-Sansegundo and Alonso, 1989; Matte, 1969). D2 deformation is recorded by the presence of upright open to tight folds generally associated with a crenulation or penetrative S2 cleavage with predominantly E-W trends and vertical dip, that generally post-dates granitic intrusions (D2 and D3 in Mezger and Passchier, 2003). Commonly, D2 deformation is mainly recorded in the Suprastructure, and is visible by the presence of numerous F2 folds and, in the Devonian rocks, probably related to detachment layers on Silurian black-schists (García-Sansegundo et al., 2011). Nonetheless, in the Infrastructure, D2 is locally recorded with tight F2 folds in Ordovician schists associated with crenulation or penetrative S2 cleavage (Cugerone et al., 2018b; Mezger and Passchier, 2003).

2.2.2. Magmatic bodies

A calc-alkaline granitoid occupies the metamorphic core (south of the Bossòst dome; Fig. 2a) and is part of a kilometric-size batholith in the northern sub-metamorphic core generating M2-LP-HT metamorphism (see cordierite spots in the Fig. 2). The granitic pluton intrudes Cambro-Ordovician metapelites and locally marble (Fig. 2B) and is essentially composed of undeformed leucocratic muscovite-hornblende granites, minor two-micas granites (Mezger and Passchier, 2003), and local plastically-deformed hornblende tonalite (Mezger and Gerdes, 2016). In the southern sub-metamorphic core, many localized granitic dykes intruding metasedimentary rocks are observed along an E-W trend (Fig. 2A and B). The folded E-W trending S1 is crosscut by the main granitic body and sub-vertical E-W S2 cleavage has probably developed at depth during the formation of the Bossòst granite (Mezger and Passchier, 2003). D2 deformation may have continued during the consolidation of the granitic body (Mezger and Gerdes, 2016).

2.2.3. Metamorphism

In the Bossòst metamorphic core, metapelites have been affected by polyphase metamorphism (Mezger and Passchier, 2003; Mezger et al., 2004). In the Infrastructure, M1 Barrovian metamorphism is recorded in staurolite and garnet schists with a peak estimated at 580 °C and 0.5 GPa. A zinc-spinel (gahnite; $ZnAl_2O_4$) locally reported in the Infrastructure, is probably associated with M1 metamorphism and is cross-cut by stratabound Pb-Zn mineralized bodies at Victoria deposit (Fig. 2A) (Cugerone et al., 2018b; Pujals, 1992). This regional metamorphism is locally overprinted by HT M2 assemblage with late syn-kinematic growth of cordierite, which constitutes a contact aureole (0.5–1 km in thickness) according to Mezger and Passchier (2003), with an estimated peak at 575–600 °C and 0.3 GPa (Fig. 2A and B). A prograde zoning with biotite, andalusite-cordierite and sillimanite-cordierite assemblages is recorded towards the contact with the granite (Lopez-Sanchez et al., 2019; Mezger et al., 2004).

2.2.4. Previous geochronological studies on metamorphic core.

Mezger and Gerdes (2016) performed a geochronological study (U-Th-Pb LA-ICPMS separate-zircon) on two granites and a deformed tonalite collected in the northern part of the Bossòst metamorphic core (Fig. 2A). The granitic samples yielded well-constrained zircon concordia ages of 338.2 ± 2.5 Ma and 336.8 ± 2.0 Ma whereas the zircons of the tonalite give a less constrained age of 347 ± 10 Ma. These Visean-Serpukhovian ages are interpreted as the emplacement age of the Bossòst granite, thus defining a minimum age for M1 Barrovian metamorphism. However, the meaning and existence of these Visean-Serpukhovian ages is still controversial (Cochelin et al., 2017a; Denèle et al., 2014; Le Bayon and Cochelin, 2020; Lopez-Sanchez et al., 2019).

Lopez-Sanchez et al. (2019) dated by LA-ICPMS U-Pb separate-zircon, an undeformed leucocratic granite collected on the northern part of the Bossòst dome and obtained a more complex history with a concordia age of 295 ± 2 Ma and along with a lower intercept age at 326 ± 3 Ma. These authors interpreted this concordia age as the early-Permian emplacement of leucogranite and the lower intercept age as evidence of an early-Carboniferous thermal event recorded in pre-Variscan zircon, confirming the existence of a Visean-Serpukhovian magmatism in the PAZ. And, the most likely age for the peak M2 HT-LP metamorphism is probably Early-Permian (Lopez-Sanchez et al., 2019).

2.2.5. Stratabound Pb-Zn mineralization

Stratabound Pb-Zn mineralization is hosted in Cambrian to Late-Ordovician metasediments from the two crustal levels, but no known structural relationship between granitic bodies and stratabound Pb-Zn mineralization is reported in the Bossòst dome. Stratabound mineralization can be hosted in high-grade metapelites such as gahnite schist in the Victoria deposit, in marble and black-schists at Bentaillou or in calc-schists in the Liat-Urets deposits (Fig. 2). In the Victoria and the Horcall deposits, south and north-east of the Bossòst dome, respectively (Fig. 2A and B), stratabound mineralization is intensely folded by F2 folds but cross-cut metamorphic mineral assemblage such as gahnite as well as hosted in shadow pressure of garnet crystals (Cugerone et al., 2018b; Cugerone et al., 2021a; Cugerone et al., 2021b, submitted). The Bentaillou Pb-Zn deposit is located in low-grade marble and schists (Fert, 1976; Zwart, 1963b) and consequently is interpreted as part of the Suprastructure. This deposit is hosted in the normal limb and hinge zone of a kilometric-size recumbent fold (Fig. 2A and C; Cugerone et al., 2018a; Cugerone et al., 2018b; García-Sansegundo and Alonso, 1989). Based on field observations, Pb-Zn mineralization is hosted in metric- to decametric-size pull-apart type structures sub-parallel to S0-S1 foliation and consequently, stratabound Pb-Zn mineralization is interpreted as syn- or slightly post-D1 (Cugerone et al., 2018b).

3. Description of dated samples

3.1. Two granitic dykes

In the southern area of the Bossòst dome and in the Infrastructure, we have performed U-Pb dating on zircon from two granitic samples (BOS32a, BOS32b) located along the Garonne river. They were collected in E-W trending metric-size granitic dykes (Fig. 2A and B), two

kilometers away of each other. Two weakly strained and unaltered leucocratic granitic bodies intrude metapelitic rocks preserving a cordierite-sillimanite assemblage (HT-LP; 575–600 °C and 0.3 GPa) (Fig. 3A). At microscopic scale, these dykes are composed essentially of quartz, alkali feldspar and muscovite, with restricted kink-bands in muscovite, and only few recrystallized quartz crystals with sub-grains indicating limited brittle-ductile deformation (see inset in Fig. 3A).

3.2. Two metapelites

The U-Th-Pb in situ dating on monazite was performed on two late-Ordovician metapelites collected in the same area, 10 m away from each other, close to the Arres de Jos village (BOS17 and BOS18). A previous P-T study by Mezger and Passchier (2003) in this area was carried out which estimates P-T conditions of the two samples at 500 °C and 0.4 GPa. An assemblage of muscovite, biotite, garnet and staurolite aligned along S1 foliation constitutes the metamorphic assemblage. In the two samples, no cordierite or andalusite crystals that could possibly indicate superimposed HT-LP (M2) metamorphism are observed (Mezger and Passchier, 2003) (Fig. 4B). BOS17 exhibits a well-preserved S1 foliation without pronounced D2 and HT-LP overprints. Biotite, garnet and centimeter-size staurolite are common indicators of the foliation S1 (Fig. 4A). BOS18 displays similar metamorphic assemblage with biotite, garnet and staurolite aligned along the S1 foliation even if few garnet and staurolite appear parallel to the crenulation cleavage S2 associated with F2 folds (Fig. 4B).

3.3. Monazite associated with Pb-Zn mineralization from the Bentaillou deposit.

In the Suprastructure of the northeastern area of the Bossòst dome, monazite included or directly associated with sphalerite was dated in-situ in stratabound Pb-Zn mineralization from the Bentaillou deposit (BEN07 sample; Fig. 3B-D and Fig. 4C). Unfortunately, no monazite grains were found in the thin sections of other Pb-Zn deposits in the Bossòst dome (Liat, Victoria, Pale Bidau). At Bentaillou, the studied sample is hosted in late-Ordovician black-schist at the uppermost part of the Bentaillou marble and was collected at the base of one of the thickest mineralized bodies. Stratabound Pb-Zn veins are essentially composed of sphalerite and galena, with gangue minerals of calcite and muscovite, and locally crosscut minor disseminated and stratiform galena, supposed syngenetic (Fig. 3C-D and Fig. 4C-E). Pluri-millimetric-size calcite crystals appear orthogonal to the vein walls with comb-texture intergrowing with sphalerite (Fig. 4C-D). Sphalerite crystals intergrow or fill empty spaces with millimetric-size needles of muscovite, the only metamorphic mineral reported in this sample. No alteration in the host-rock is observed. Nonetheless, Bentaillou sphalerite seemed to have undergone recrystallization with presence of polygonal crystals or "foam textures" (Fig. 4C) contemporaneous of a

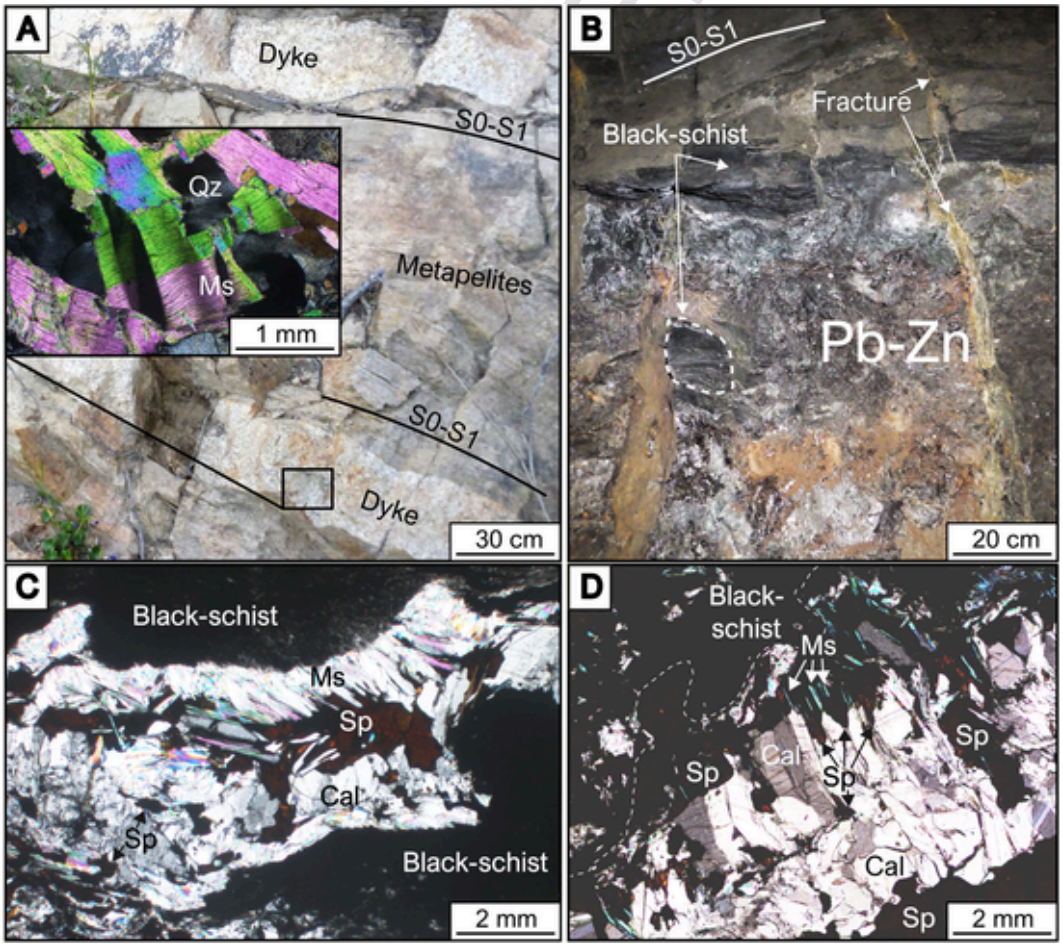

Fig. 3. Outcrop photographs and thin section microphotographs. A. Granitic dykes in the Bossòst metamorphic core crosscutting S0-S1 foliation. Small inset evidences the presence of kink bands in muscovite and relative weak recrystallization and deformation in these granitic dykes. B. Typical Bentaillou Pb-Zn mineralization hosted between Cambro-Ordovician marble and late-Ordovician black schist (1875 level – Saint-Jean gallerie). Clast of schist are observed in the Pb-Zn mineralization. C-D. Textural co-genetic relationship between sphalerite (Sp), muscovite (Ms) and calcite (Cal)in stratabound vein mineralization hosted in black-schist at Bentaillou.

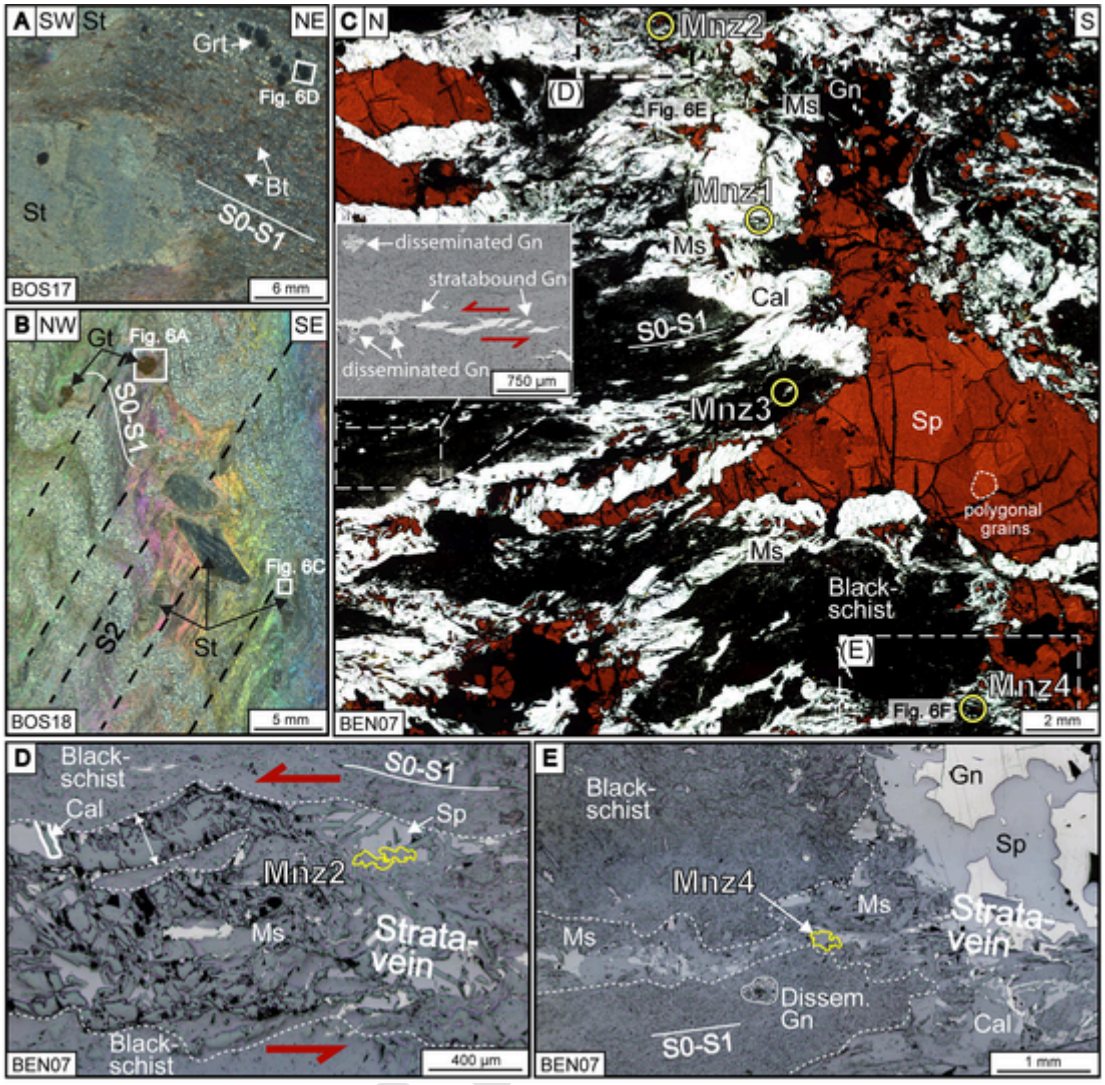

Fig. 4. A. Metapelite (BOS17) with biotite (Bt), garnet (Gt) and staurolite (St) assemblages (plane polarized light). Location of the Fig. 6D is noted with a white square. B. Metapelite (BOS18) with muscovite (Ms), garnet (Gt) and staurolite (St) assemblages (plane polarized light). Location of the Fig. 6C is represented with a white square. C. Typical sphalerite (Sp) mineralization observed in transmitted light from the Bentaillou deposit hosted in black-schist and associated with calcite (Cal) and galena (Gn). Location of the monazite crystals (Mnz) analyzed in this area are represented with yellow circle. A small inset in reflected light shows that main stratabound Pb-Zn mineralization crosscut minor disseminated galena, supposed syngenetic. D-E. Reflected light microphotographs showing the location of the Mnz2 and Mnz4 in the stratabound Pb-Zn veins. Monazite grains (Mnz) are represented in yellow and white dashed lines evidence boundaries of stratabound vein, mostly composed of sphalerite (Sp), galena (Gn) and muscovite (Ms). (For interpretation of the references to colour in this figure legend, the reader is referred to the web version of this article.)

low-grade metamorphism (< 400 °C, Cugerone et al., 2021a). Low trace contents in Ga, Ge and In (< 10 ppm) observed in the same sphalerite sample at Bentaillou is also a supporting clue of this metamorphic imprint (Cugerone et al., 2021a; Frenzel et al., 2016).

4. Instrumentation and analytical methods

Zircon crystals were obtained by a conventional mineral separation. The selected grains were mounted on 2.5 cm blocks with epoxy resin and polished. Monazite was analyzed in-situ in thin section in order to preserve the textural relationships between monazite, sphalerite and the metamorphic minerals. Before analysis, backscatter electron (BSE) and cathodoluminescence (CL) images were acquired for all grains using a scanning electron microscope (SEM) in order to check spot positions with respect to the internal microstructures, inclusions, fractures and physical defects.

U-Th-Pb geochronology of zircon and monazite was conducted by laser ablation inductively coupled plasma spectrometry (LA-ICPMS) at Laboratoire Magmas & Volcans (Clermont-Ferrand, France). The analyses involved the ablation of minerals with a Resonetics Resolution Excimer laser system operating at a wavelength of 193 nm. The detailed analytical procedures are described in Paquette et al. (2014) and detailed in Hurai et al. (2010) and in the supplementary material (ESM1). Data reduction was carried out with the software package GLITTER® from Macquarie Research Ltd (Jackson et al., 2004; Van Achterbergh et al., 2001). Calculated ratios were exported and ages and diagrams were generated using the Isoplot/Ex v. 2.49 software package of Ludwig (2001). The decay constants used for the U-Pb system are those determined by Jaffey et al. (1971) and recommended by the IUGS (Steiger and Jäger, 1977). In the text, figures and supplementary materials, all uncertainties in ages are given at $\pm 2\sigma_{level}$.

5. U-Th-Pb results

5.1. Zircon dating of two granitic dykes

Zircons in the two Bossòst granite dykes are rare, medium sized (between 100 and 200 μm), and often metamict (see ESM2).

Sample BOS32b shows two distinct zircon populations. One is opaque red with numerous inclusions of UO_2, biotite and quartz. The second is slightly more translucent showing euhedral crystal with bipyramidal shape and generally rare inclusions. Moreover, some grains have a thin rim (~10 μm) rich in inclusions. Only the second population could be dated. Cathodoluminescence is low and displays a slight oscillatory zoning (ESM2). A total of 28 spots on 24 crystals was performed and plotted on the concordia diagram (Fig. 5A; ESM3). These analyses show very low Th/U ratios (≪0.1; ESM3) associated with low Th (1.1–6.7 ppm), high to very high U (3624–20918 ppm) and

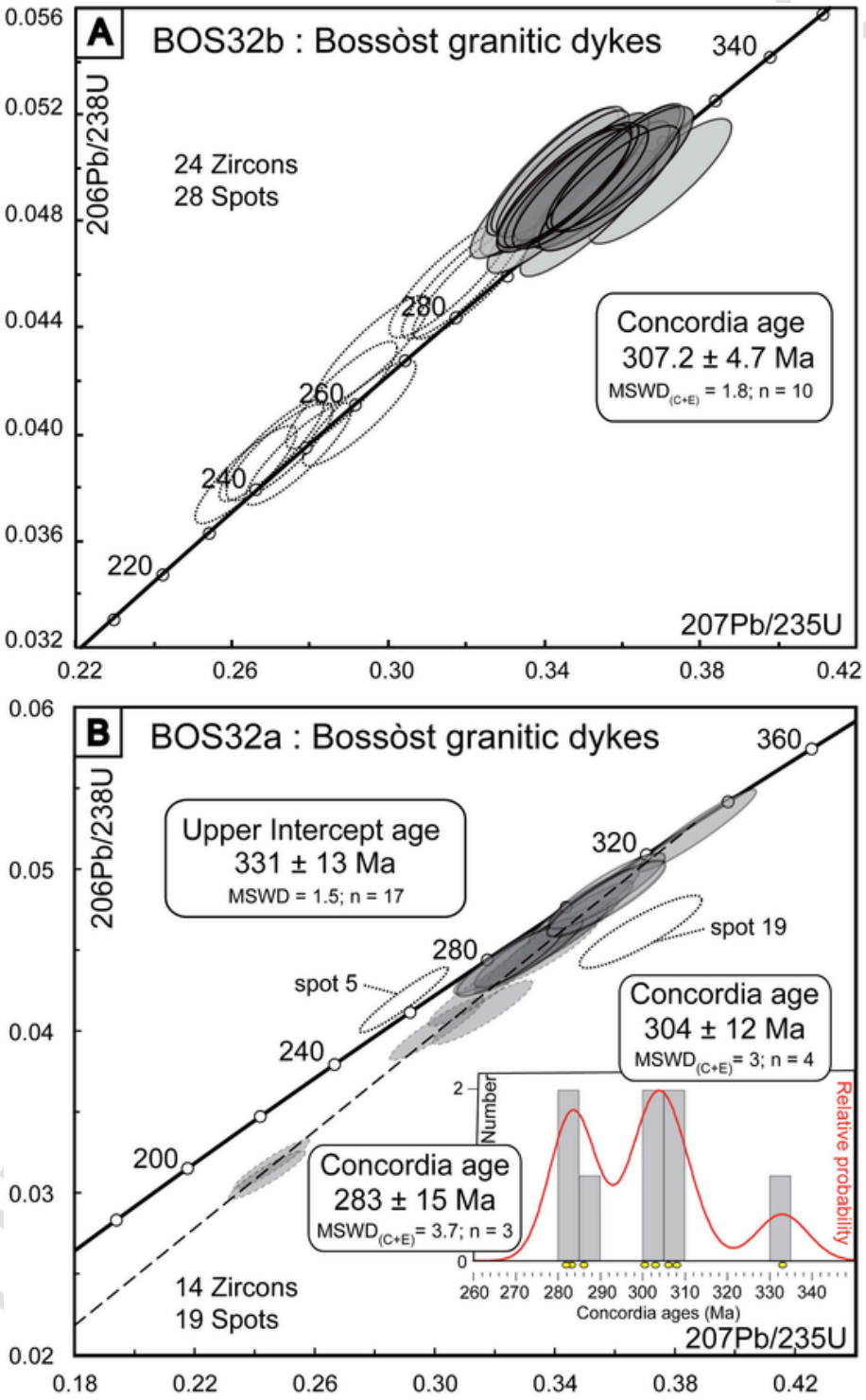

Fig. 5. A. and B. Zircon U-Pb concordia diagrams (LA-ICP-MS) obtained on two granitic dykes of the Bossòst metamorphic core, BOS32B and BOS32A, respectively. Error ellipses and uncertainties in ages are ± 2σ. The stippled ellipses are not taken into account for the age calculation. "n" corresponds to the number of data used to calculate the age. Histogram distribution diagrams is shown. To avoid distorting the distribution of populations, only one date per grain is used.

medium–high Pb concentrations (165–930 ppm). The 28 ellipses are concordant to sub-concordant between 230 and 330 Ma. Among these analyses, 18 ellipses constitute a cluster around 310 Ma yielding a concordia age of 307.2 ± 4.7 Ma ($MSWD_{(C+E)}$ = 1.8; n = 10) and 10 analyses represented by dotted ellipses, performed on zircon rims, present younger ages. These data are not taken into consideration for the age calculation because they reflect probably radiogenic Pb losses.

In the BOS32a sample, most of the zircons are fragments (ESM2). No internal structure is identified, and grains contain many fractures and inclusions of UO_2 and biotite. A total of 19 analyses, carried out on 14 crystals are listed in the ESM3 and plotted in Fig. 5B. Except for spots 1 and 5, the data show low Th (1–7 ppm), high U (3119–13398 ppm) and medium Pb concentrations (140–539 ppm). Their Th/U ratios are very low (≪0.1; ESM3). The concordia diagram shows a more complex date pattern showing a great dispersion of $^{206}Pb/^{238}U$ dates between 330 and 200 Ma and with only a small number of concordant ellipses (n = 8) (Fig. 5B; ESM3). Usually, the discordant data analyzed by the LA-ICPMS method are only considered if they allowed possible discordia line to be defined by a linear regression on the concordia diagrams; otherwise they are not taken into consideration because of doubtful interpretation. Nonetheless, several factors that cannot be easily detected from the inspection of the time-resolved signals might contribute to discordance such as common Pb related to low U content inclusions, mixing of different age domains or presence of small cracks. A linear regression of 17 analyses (excepted spot 5 and 19) yields an upper intercept of 331 ± 13 Ma (MSWD = 1.5). But if we consider only the eight data with single-grain concordia age, the dates histogram shows the presence of three populations at ~330 Ma (group 1), ~305 Ma (group 2) and ~285 Ma (group 3) (Fig. 5B; ESM3). Group 1 is recorded by one zircon (Z1) with a concordia age of 333 ± 12 Ma. This analysis differs from the others by its Th content (29 ppm). Group 2 is determined from 3 crystals (Z10, Z15 and Z16). These data yield a concordia age of 304 ± 12 Ma ($MSWD_{(C+E)}$ = 3; n = 4). The last group is also composed of 3 zircon crystals and yields a concordia age of 283 ± 15 Ma ($MSWD_{(C+E)}$ = 3.7; n = 3). The other data are interpreted as reflecting the presence of a slight Pb loss (dotted grey ellipse) together with the probably small amount of common Pb (spot 19).

5.2. Monazite dating of two metapelites

Monazite from two metapelites (BOS17 and BOS18) range from 10 to 200 μm with an irregular outline. These grains appear either parallel to foliation S1 or cleavage S2, or included in metamorphic mineral assemblages such as garnet, staurolite or muscovite in BOS18 (Fig. 6A-C) and staurolite in BOS17 (Fig. 6D). Monazite is homogeneous, without internal zoning patterns in Ce, Y or Th. In BOS18 and BOS17 samples, 19 and 11 spots were performed on 11 and 5 monazite crystals respectively (ESM3). The analyses of both samples are similar with a wide range of Th (most 2 000–46 500 ppm), U (100–3 200 ppm) and Pb (most 180–1380 ppm) concentrations and the ratio Th/U is relatively low (4.6–31). In the concordia plots, the ellipses of both samples plot between 280 and 330 Ma with a concordant cluster around 290 Ma and some discordant data probably related to common Pb contaminations (Fig. 7A and B). The linear regression for the samples BOS17 and BOS18 yields a lower intercept of 289.1 ± 5.9 Ma (MSWD = 0.1; n = 10) and 290.0 ± 3.8 Ma (MSWD = 0.1; n = 18), respectively. There is no relation between monazite included in metamorphic mineral assemblages or hosted in matrix (ESM3). Nonetheless, for the BOS17 sample, two analytical spots on one monazite crystal included in garnet near a fracture (Mnz7) exhibit significant differences in age (ESM3 and Fig. 6D). This analysis close to the fracture yields a date of 294 ± 13 Ma, and in a distant from the fracture a date of 329 ± 14 Ma (spots # 9 and 10; Fig. 6D). For the sample BOS18, the analytical spot (# 15) carried out on a monazite included in staurolite yields a $^{206}Pb/^{238}U$ date of 334 ± 13 Ma (Fig. 6C). The dates obtained by lower intercept for the both samples (BOS17 and BOS18) are similar (289.1 ± 5.9 Ma and 290 ± 3.8 Ma). If we plot all the data in a same diagram, we obtain a lower intercept date of 289.8 ± 3.0 Ma (MSWD = 0.1; n = 28) and two older data around 330 Ma showing a slight discordance probably due to a low common Pb contamination (ESM3, Fig. 7C). If we report these two data on the common-Pb composition of the two-stage crustal evolution model of Stacey and Kramers (1975), two similar single-grain concordia ages with common-corrected Pb yield 329 ± 7 Ma (# 14; BOS18) and 326 ± 7 Ma (# 10; BOS17).

5.3. Monazite dating associated with Pb-Zn mineralization from the Bentaillou deposit.

At Bentaillou, monazite crystals have anhedral shapes (BEN07 sample; Fig. 4C-E and Fig. 6E-F), sometimes fragmented with usually irregular and resorbed edges. They are systematically associated with a micrometric-size muscovite corona of various thickness (<50 μm). The studied monazite and muscovite assemblage is found in textural contact or included into sphalerite (Fig. 6E and 6F). Inclusions of galena, sphalerite, muscovite, and ilmenite are observed in monazite (<10 μm; Fig. 6E and F). Monazite is not clearly zoned in Ce, Y and Th. In the BEN07 thin section, 10 spots were performed on 5 monazite crystals (ESM3; Fig. 8). The studied monazites have a large range of Th (1 087–9 700 ppm), U (215–964 ppm) and medium Pb concentrations (142–432 ppm) with a low Th/U ratio (1.6–28.3). The results are plotted in a Tera-Wasserburg diagram because the data are very discordant due a relatively high proportion of common Pb (Fig. 8). The linear regression yields a lower intercept of 309 ± 11 Ma (MSWD = 1.6; n = 10) and a 207Pb/206Pb initial value of 0.869 ± 0.054 consistent with the composition of the Variscan common Pb (c.a. 0.856) following the model of Stacey and Kramers (1975) for the terrestrial Pb evolution.

6. Discussion

6.1. Ages interpretation

6.1.1. Zircon dating of two granitic dykes

In the Infrastructure of the southern area of the Bossòst dome, the two low strain unaltered leucocratic granite dykes exhibit identical textural and petrogenetic patterns. Zircon Th/U ratios and U contents are typical from peraluminous granitoids and particularly the early-Permian leucocratic granite facies of the Bossòst pluton (Lopez-Sanchez et al., 2019; Lopez-Sanchez et al., 2016). The first sample (BOS32b) shows a cluster of data with a concordia age of 307.2 ± 4.7 Ma, which is interpreted as the emplacement age of this granitic dyke. This age is in agreement with the commonly reported ages for Late-Variscan magmatism within the PAZ generally ranging between 315 and 300 Ma (Figs. 1 and 9; e.g. Denèle et al., 2014).

Due to a large spread of the data along the concordia line, the interpretation of the second sample (BOS32a) is more complex. The dates histogram shows the presence of three zircon populations (Fig. 5B). The concordia age of 283 ± 15 Ma obtained on the youngest zircon population may be interpreted as the emplacement age of this dyke. This poorly constrained age is similar within error to the emplacement age at 295 ± 2 Ma from the undeformed leucocratic granite collected on the western edge of the main Bossòst batholith (Lopez-Sanchez et al., 2019) (Fig. 2A). Moreover, early Permian magmatic intrusions (298–290 Ma) are widespread throughout the whole PAZ (Druguet et al., 2014; Kilzi et al., 2016; Lemirre et al., 2019; Lopez-Sanchez et al., 2019; Poitrenaud et al., 2019; Schnapperelle et al., 2020; Van Lichtervelde et al., 2017). Recently, Schnapperelle et al. (2020) have proposed that the leucocratic granite dykes intruding the Aston and Hospitalet domes were also emplaced in the late-Carboniferous to early-Permian as well (ca. 306–297 Ma). These dykes preserve abundant xenocrysts and inherited zircon grains that are preserved from the

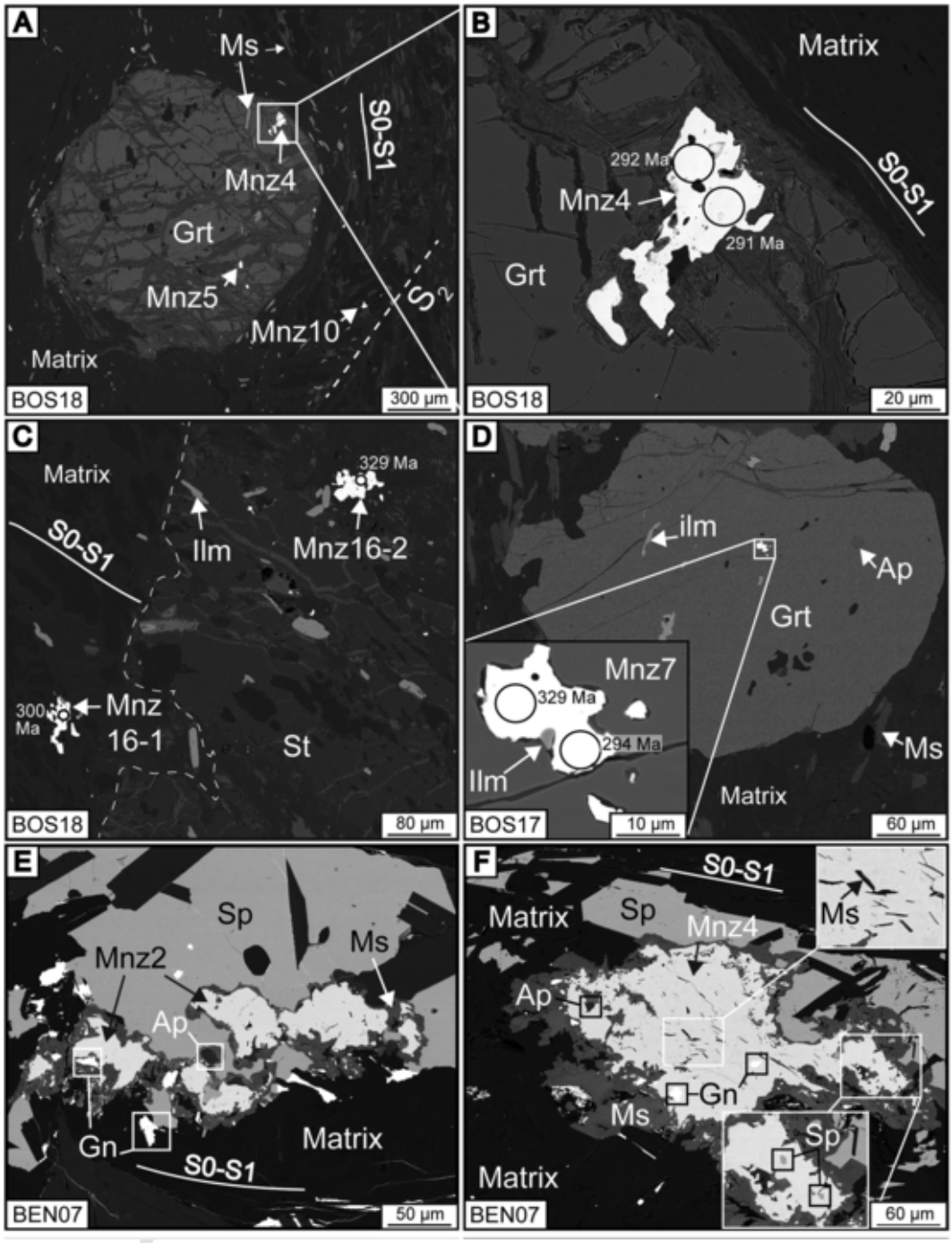

Fig. 6. Back-scattered electron (BSE) images of the studied monazites. Age (Ma) and location of LA-ICP-MS analyses are shown in A-D (abbreviations: Ap: apatite; Gn: galena; Gt: garnet; Ms: muscovite; Mnz: monazite, St: staurolite). A. Monazites included in garnet (Mnz 4, 5 and 10; BOS18). B. Zoom of the monazite Mnz4 (Concordia age; BOS18). C. Monazite associated with staurolite (Mnz16-1 and 16–2 with $^{206}Pb/^{238}U$ ages; BOS18). D. Monazite included in garnet and associated with ilmenite and close to a fracture (Mnz7 with Concordia ages; BO17). E. Monazite assemblage associated with sphalerite and muscovite (Mnz2, BEN07). F. Monazite associated with sphalerite with inclusions of muscovite and galena (Mnz4; BEN07).

melt of the dykes. This suggests the recycling and incorporation of material of the adjacent intruded rocks during magma ascent through the crust (Schnapperelle et al., 2020).

This may also explain the presence of the other two older populations obtained in the BOS32a sample. One population yields a concordia age of 304 ± 12 Ma, which is similar to the one obtained within error to the first dyke (BOS32b). The other population at 333 ± 12 Ma (Fig. 5B) is consistent with the Visean concordia ages (ca. 337–339 Ma) interpreted as the emplacement age of the Bossòst granitic dome by Mezger and Gerdes (2016). Moreover, close to the study area, Visean detrital zircons of igneous origin have been reported from Serpukhovian Culm flysch deposits in the Aran valley, south of the Bossòst dome which infer the probable presence of Visean magmatic bodies at the surface during flysch sedimentation (Martínez et al., 2016) (Fig. 2).

6.1.2. *Monazite dating of two metapelites*

The dating of monazite included or not in metamorphic minerals yields similar lower-intercept dates at 289.1 ± 5.9 and 290 ± 3.8 Ma, respectively. There is no significant difference in age between the various textural positions (e.g., inclusion vs. matrix) or structures (S1 or S2)

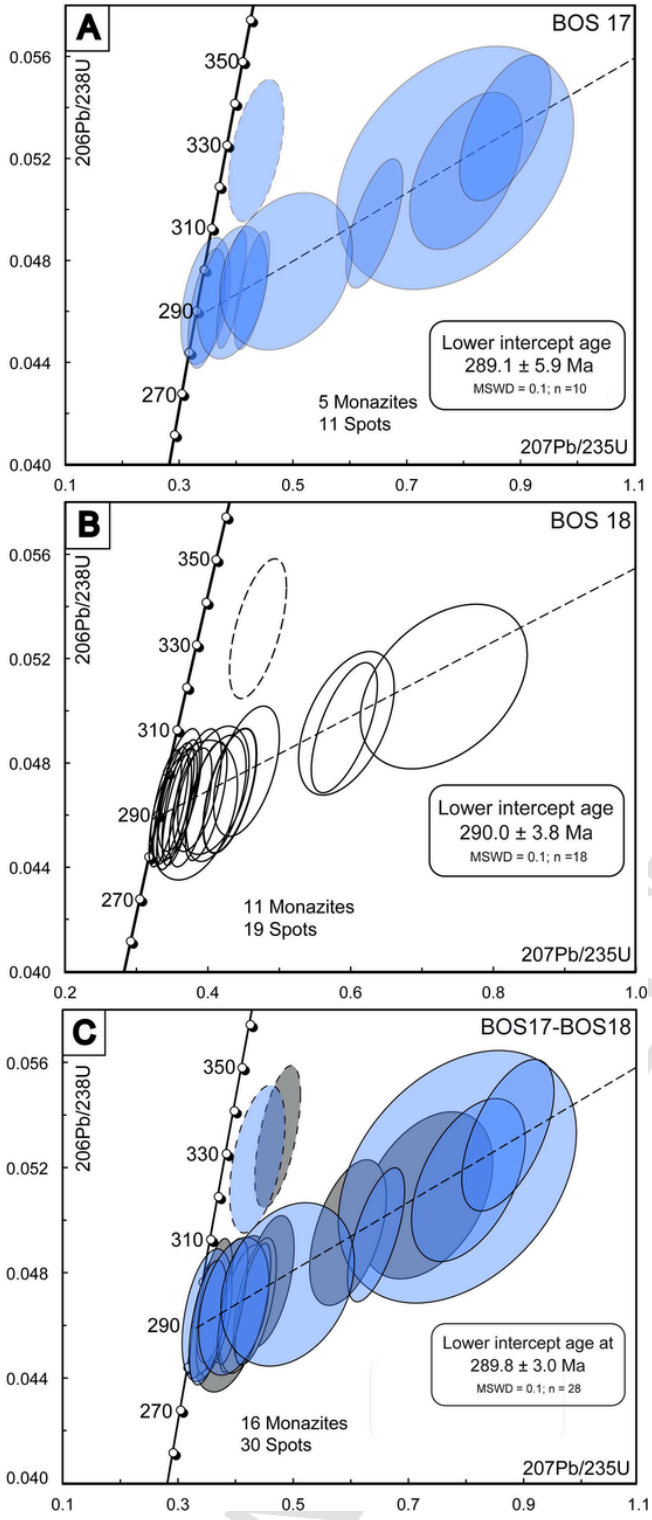

Fig. 7. U-Th-Pb concordia diagrams for the monazites analyzed in the metapelites. Error ellipses and uncertainties in ages are ± 2σ. The stippled ellipses are not taken into account for the age calculation. A. Monazites from BOS17. B. Monazites from BOS18 and C. Monazites from BOS17 and BOS18.

except with two sub-concordant data points recording older dates at ~330 Ma. These were obtained on monazite grains included in a garnet (#10 of BOS 17) and in a staurolite (#14 of BOS 18) (Fig. 7), and in domains with no brittle fracture and probably preserved from fluid circulation. Generally, monazite preserve crystallization ages because it is not sensitive to Pb diffusion (e.g. Cherniak et al., 2004; Gardés et al., 2007; Seydoux-Guillaume et al., 2002) but monazite is prone to recrystallize due to dissolution/precipitation processes when fluids or melts are involved, and the isotopic system may therefore be partially or totally reset (e.g. Bosse et al., 2009; Didier et al., 2014; Hetherington et al., 2010; Kelly et al., 2012; Rasmussen and Muhling, 2007; Tartèse et al., 2011; Williams et al., 2011). Our monazite ages on metapelites show two Variscan episodes of monazite growth: one of Visean-Serpukhovian age (~330 Ma), and the other of early-Permian age (~290 Ma). These two episodes are likely to coincide with the two magmatic events (340–325 Ma and 310–295 Ma) described in the Bossòst dome (Lopez-Sanchez et al., 2019; Mezger and Gerdes, 2016) and more generally in the PAZ (e.g. Denèle et al., 2014; Schnapperelle et al., 2020) (Fig. 1B, 9 and ESM3).

These data confirm this diachronism in ages already observed for magmatic and metamorphic rocks (Aguilar et al., 2015; Aguilar et al., 2014; Esteban et al., 2015; Lopez-Sanchez et al., 2019; Mezger and Gerdes, 2016). Most of these authors agree that the dominant HT-LP metamorphism was contemporaneous with a widespread magmatic event that occurred between 315 and 290 Ma. We interpret the early Permian ages of c.a. 290 Ma recorded by monazites from the Bossòst metapelites as their recrystallization ages due to the upward percolation of late-anatectic melts as well as the fluid–rock interaction during the late-stage HT-LP (M2) metamorphic history recorded in the Bossòst metamorphic core. The two older ages at ca. 330 Ma may be linked to the early MP-HT (M1) metamorphic episode. Even if additional data are needed to validate the age of this event, these data are similar in error limits to the Visean ages obtained on Bossòst and Aston dome (Lopez-Sanchez et al., 2019; Mezger and Gerdes, 2016).

6.1.3. Monazite dating associated with Pb-Zn mineralization from the Bentaillou deposit.

Monazite grains hosted in the Bentaillou stratabound Pb-Zn veins parallel to S1 foliation yield an age of 309 ± 11 Ma. At Bentaillou, the studied monazite grains are always found within stratabound Pb-Zn veins and contain inclusions of galena and sphalerite. No metamorphic or alteration mineral is reported close to the Pb-Zn mineralization except muscovite associated or included into sphalerite and monazite. Their irregular shape, relative coarse grain size (up to ~100 μm) and association with muscovite may be related to precipitation of monazite under low-grade metamorphic conditions (< 400 °C; (Milodowski and Zalasiewicz, 1991; Rasmussen et al., 2001; Rasmussen and Muhling, 2007; Wilby et al., 2007; Wing et al., 2003). Nonetheless, textural and chemical observations seem to indicate static recrystallization only in sphalerite, with coarse "foam" texture (Cugerone et al., 2021a). Sphalerite is commonly considered as a ductile mineral and can recrystallize at low-temperature under experimental conditions (< 400 °C; Cugerone et al., 2020; Kelly and Clark, 1975; Kollenberg and Siemes, 1983; Siemes et al., 1991; Siemes and Hennig-Michaeli, 1985). Based on fieldwork observations and textural evidence between monazite, muscovite and sphalerite, we consider the data of 309 ± 11 Ma as the age of stratabound Pb-Zn mineralization formation during a major Variscan remobilization event, which is clearly synchronous to the main magmatic-metamorphic event reported in the metamorphic core of the Bossòst dome (310 Ma). This is the first geochronological evidence of Variscan Pb-Zn mineralizing event in the Pyrenees. This is consistent with the field work arguments of Cugerone et al. (2018a) and Cugerone et al. (2018b) in the Bentaillou mining district. Therefore, the formation of stratabound Pb-Zn mineralization may be synchronous to D1 deformation associated with MT-MP regional metamorphism in the Suprastructure and synchronous to the Late-Carboniferous magmatism (310–300 Ma).

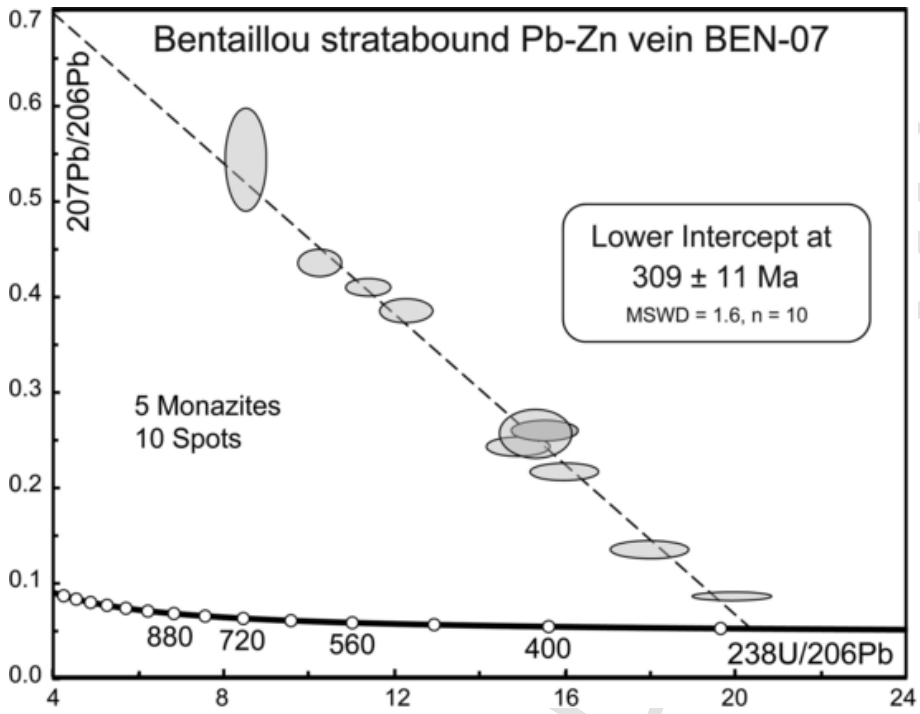

Fig. 8. U-Th-Pb concordia diagrams for the monazites associated with sphalerite from the Bentaillou deposit. Error ellipses and uncertainties in ages are ± 2σ. The stippled ellipses are not taken into account for the age calculation.

6.2. *Timing of magmatic and metamorphic events in the Bossòst dome*

In the PAZ, the transition between MT-MP and HT-LP metamorphism is considered Late-Carboniferous (308 Ma) according to Denèle et al. (2014) but this geodynamic model does not take into account the Visean-Serpukhovian magmatism recently reported in the literature (Mezger and Gerdes, 2016; Schnapperelle et al., 2020). Moreover, this transition has been newly reported at 340–335 Ma due to the presence of Visean magmatism (340–320 Ma) in the Infrastructure and further migmatization of these plutons during HT-LP metamorphism recorded by monazite in the Aston dome (325 Ma; Mezger and Gerdes 2016). At the same period, a transition between thickening of the crust (D1) and doming (D2) is proposed (Mezger and Gerdes, 2016) In the Suprastructure, magmatism is restricted to Late-Carboniferous and HT-LP metamorphism is very limited.

In our study, zircon and monazite ages on leucogranite dykes and metapelites mainly record a Late-Carboniferous age (310–290 Ma) for Variscan magmatism and metamorphism. Nonetheless, data obtained on monazite hosted in staurolite and garnet as well as one zircon show the occurrence of a Visean-Serpukhovian magmatism and metamorphism event (330 Ma; Fig. 9). Meanwhile, our monazite age of 309 ± 11 Ma recording the formation of syn-D1 Pb-Zn mineralization at Bentaillou is difficult to reconcile with the D1-D2 transitions (340–335 Ma) proposed by Mezger and Gerdes (2016) in the Bossòst dome. As a consequence, we suggest that deformation and metamorphism were decoupled between the two structural levels (Fig. 10), similar to the model of Carreras and Capella (1994). Consequently, we interpret the tectono-metamorphic evolution that frames the stratabound Pb-Zn mineralizing event as follows:

At 340 Ma, the first tectonic event recorded in the two structural levels of the Bossòst dome is a long-lived period of D1 thickening, identified by kilometric-scale folding and thrusting (Fig. 10). These structures are mainly observed in the low-metamorphic Suprastructure, but are assumed to be present in the Infrastructure as well (García-Sansegundo and Alonso, 1989; Matte, 2002; Matte, 1969). During D1, MT-MP metamorphism (M1) occurs in the Bossòst Infrastructure (Mezger and Passchier, 2003). Between 340 and 330 Ma, Visean-Serpukhovian peraluminous magmatism (Figs. 9 and 10) occurs as a consequence of crustal thickening. Plutons intrude the Infrastructure core and the central part of the PAZ (Mezger and Gerdes, 2016). In the south of the Bossòst dome, the oldest fossils discovered in the flysch basins attest that the deposition of sediments is late-Visean-Serpukhovian. Undeformed granites that crosscut foliated flysch sediments in basins between 305 and 295 Ma allow to provide a minimum age for the end of sedimentation (e.g. 302 ± 7 Ma for Maladeta granite in the Aran Valley). Moreover, clasts of Visean-Serpukhovian deformed granite are found in flysch basins (e.g. 338 ± 2 Ma in the Aran Valley), demonstrating that these granites were at least partially eroded at that time (Martínez et al., 2016). In the Suprastructure, no Visean-Serpukhovian magmatism is known but a low-grade regional metamorphism, certainly related to M1 metamorphism is reported (Cugerone et al., 2018b). It remains generally poorly recorded in the PAZ (Cochelin et al., 2017b; de Hoÿm de Marien et al., 2019; Mezger and Gerdes, 2016).

Between 310 and 290 Ma, the main Late-Carboniferous magmatism occurs with the emplacement of kilometric-scale batholiths in all the PAZ. It is related to a regional temperature increase following crustal thickening and partial melting in the lower crust (Vilà et al. 2007; Carreras and Druguet 2014; Denèle et al. 2014; Fig. 10). In the Suprastructure, magmatism is limited even if some undated leucocratic granite intrusions are locally reported at the north-western part of the Bossòst dome (Fig. 2A). During this stage (310 Ma), D2 simple shear deformation develops in the Infrastructure and the Suprastructure, generally dominated by tight F2 folds. These have deformed and locally remobilized stratabound Pb-Zn mineralization in fold hinge or D2 thrusts. In the Infrastructure, a HT-MP metamorphism (Fig. 9) lead to the formation of cordierite(- andalusite) assemblage with weak occurrence of staurolite and local migmatite formations, mainly reported close to the Bossòst magmatic bodies (Mezger and Passchier 2003; Fig. 2).

At 290 Ma, during the collapse of Variscan orogen, leucocratic granite dykes intrude and are associated with late-magmatic fluids percolation (Fig. 10). D2 deformation ends and is locally reported in the Infrastructure. Frequent upright and tight E-W folds, certainly related to D2, are observed in the Suprastructure as well (Fig. 10). The E-W Bossòst

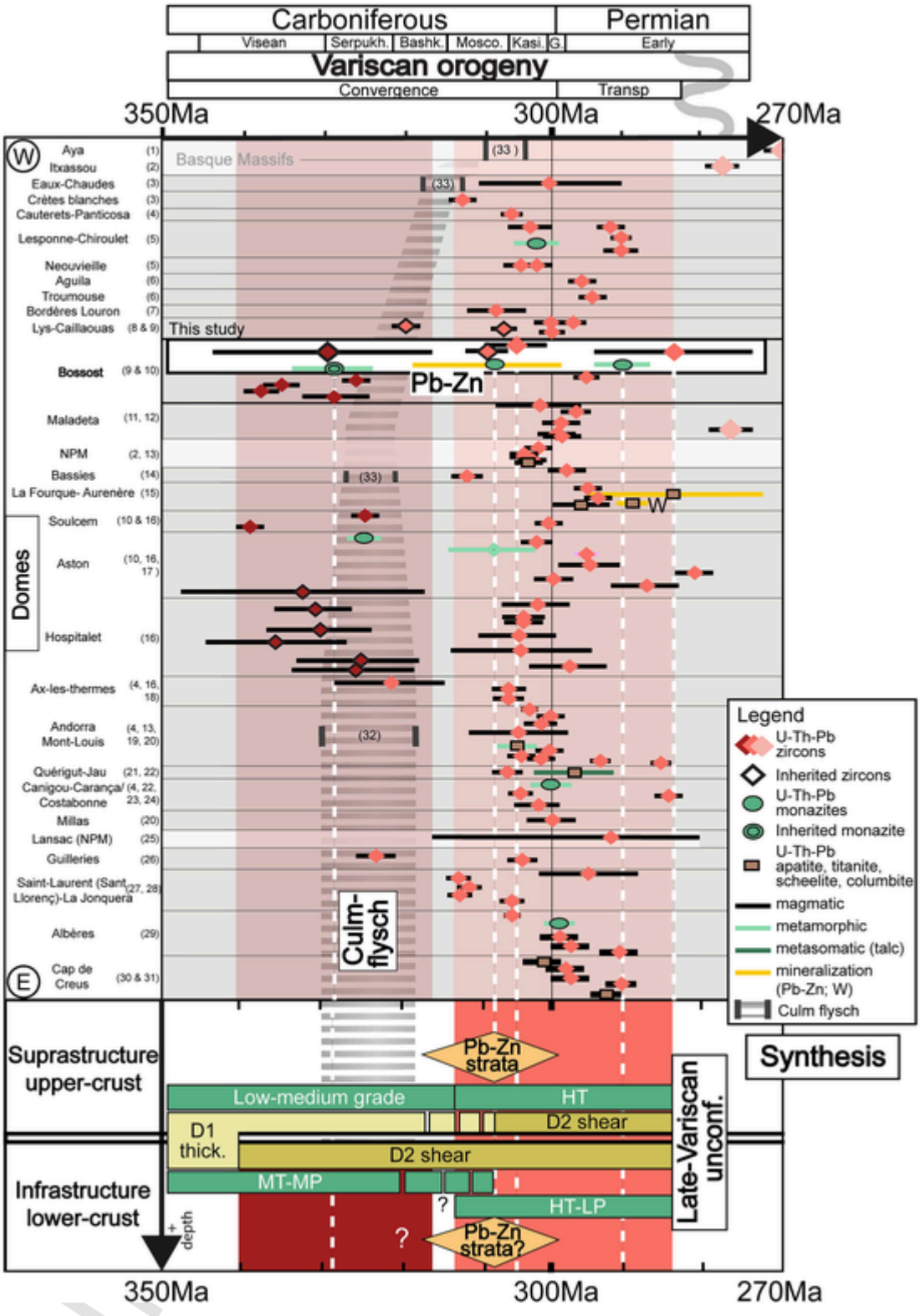

Fig. 9. Chronological succession of the magmatic, metamorphic and Pb-Zn mineralization events in the Pyrenean Axial Zone (PAZ) and in the North Pyrenean Massifs (NPM). The ages are disposed according to an E-W transect. The two Variscan magmatic events are evidenced. Timing of metamorphic, deformation and mineralization ages is proposed in the bottom part (Complete dataset in the ESM3). References: (1) (Denèle et al., 2012); (2) (Vacherat et al., 2017); (3) (Ternet et al., 2004); (4) (Denèle et al., 2014); (5) (Lemirre et al., 2019); (6) (Kilzi et al., 2016); (7) (Gleizes et al., 2006); (8) (Esteban et al., 2015); (9) ((Lopez-Sanchez et al., 2019); (10) (Mezger and Gerdes, 2016); (11) (Martínez et al., 2016); (12) (Pereira et al., 2014); (13) (Fallourd et al., 2014); (14) (Paquette et al., 1997); (15) (Poitrenaud et al., 2019); (16) (Schnapperelle et al., 2020); (17) (Lemirre, 2018); (18) (Denèle et al., 2007); (19) (Maurel et al., 2004); (20) (Romer and Soler, 1995); (21) (Roberts et al., 2000); (22) (Boutin et al., 2016); (23) (de Hoÿm de Marien et al., 2019); (24) (Laumonier et al., 2015); (25) (Poujol et al., 2010); (26)

(Martínez et al., 2008); (27) (Maurel, 2003); (28) (Aguilar et al., 2014); (29) (Laumonier et al., 2013); (30) (Druguet et al., 2014); (31) (Van Lichtervelde et al., 2017); (32) (Martín-Closas et al., 2018); (33) (Delvolvé et al., 1998).

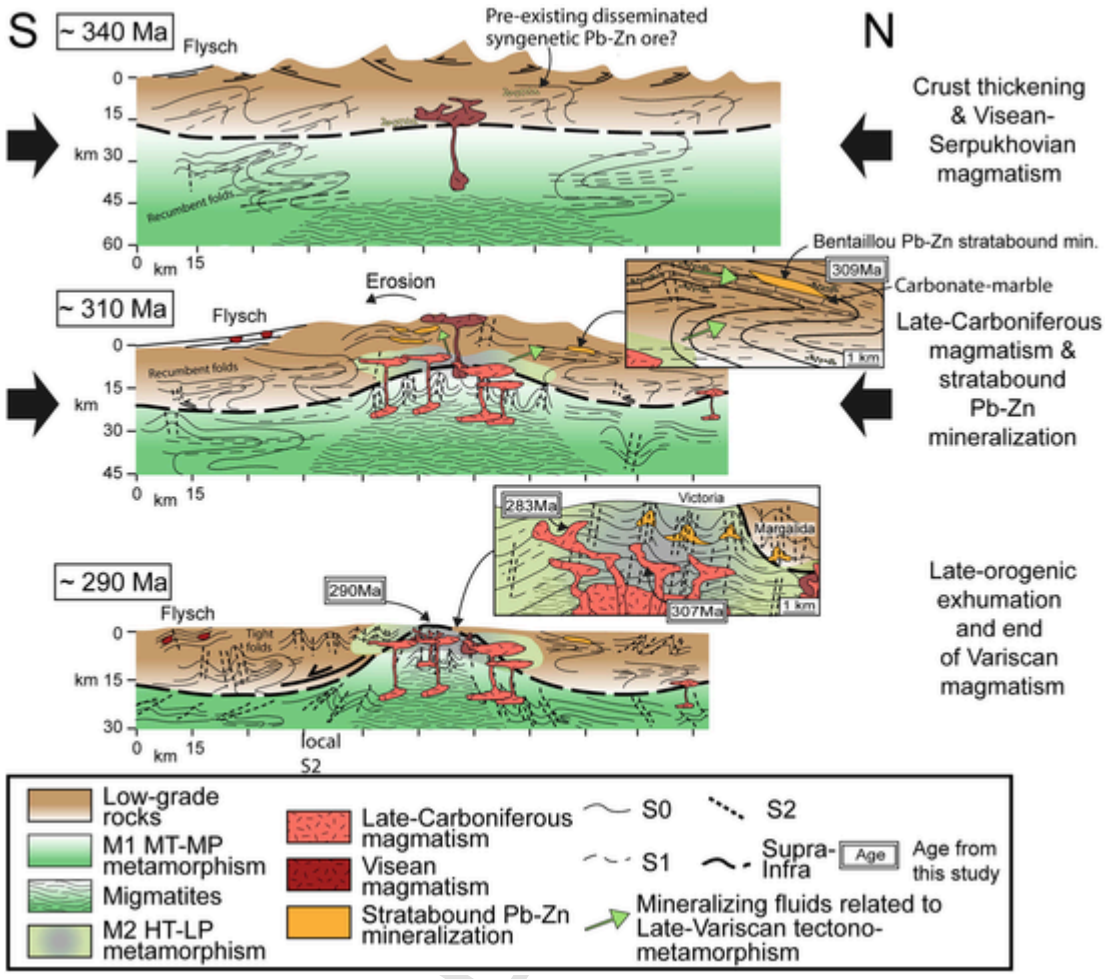

Fig. 10. Three stage geodynamic model of the Bossòst dome with two small insets representing reconstitution sketches based on field observations and metamorphic, magmatic and Pb-Zn mineralization ages of this study. At 340 Ma, crustal thickening associated with large recumbent F1 folds is represented and crustal melting starts in the Infrastructure leading to local occurrence of Visean-Serpokhovian magmatism. A regional M1 MT-MP metamorphism impacts mostly the Infrastructure. At 310 Ma, general hot Infrastructure, thicker in the central part of the Bossòst dome, causes significant crustal melting and production of Late-Carboniferous magmatism during an intense period of simple-shear D2 deformation in the Infrastructure. M2 HT-LP metamorphism is essentially related to the increase of temperature, close to the ascending Late-Carboniferous batholiths. At this stage, stratabound Pb-Zn mineralization (in orange) are represented in the two structural levels, probably related to Late-(Carboniferous magmatism and trapped in specific structures (upper flank of F1 recumbent folds, lithological interferences, etc.). At 290 Ma, late-orogenic exhumation is represented with final magmatism associated with leucocratic granite dykes and deformation of stratabound Pb-Zn mineralization. (For interpretation of the references to colour in this figure legend, the reader is referred to the web version of this article.)

fault is probably Late-Variscan to Mesozoic in age following the observation of polygenic breccia with undeformed granitic clasts close to the Margalida stratabound Pb-Zn mineralization (Figs. 2 and 10; Cugerone et al., 2018b).

6.3. Relationships between orogenic events and Pb-Zn mineralization

The late-Carboniferous monazite age (309 ± 11 Ma) of the Bentaillou stratabound sphalerite is not in agreement with an Ordovician *syn*-sedimentary SEDEX type mineralization formation, which was initially proposed for all stratabound Pb-Zn ores in the PAZ (Pouit, 1986; Pouit, 1978). Indeed, lead isotopic compositions previously obtained on galena from various PAZ deposits have suggested a common upper crustal lead reservoir. The extraction of base metals, probably from the metamorphic basement by hydrothermal fluids has been considered late-Ordovician-early Devonian in age, synchronous to the extensional event(s) (García-Sansegundo et al., 2014; Marcoux et al., 1991; Nicol et al., 1997; Cardellach et al., 1996). Nonetheless, in this study, Type 1 disseminated sphalerite and galena in Ordovician levels, initially interpreted as syngenetic and pre-Variscan in age, is crosscut by the main Pb-Zn stratabound mineralization. This suggests a more complex history associated with significant Variscan sulfide remobilization, probably from a primary Ordovician metal source (Fig. 4C; Cugerone et al., 2018b). Accordingly, it seems that the sphalerite-galena recrystallization and mobilization do not affect the lead isotopic composition. Thus, the Ordovician model ages date the first sphalerite-galena crystallization.

In the Bossòst dome, stratabound Pb-Zn veins generally present similar structural characteristics with close association with S1 foliation: the Liat Pb-Zn ore deposit is strictly parallel to S1 foliation and locally crosscuts S0 stratification (Cugerone et al. 2018b; Fig. 2A). In the Horcall and Urets deposits, sphalerite is locally observed in pressure shadows of M1 garnets even if the stratabound ore is frequently affected by D2 tectonics (Alonso 1979; Cugerone et al. 2018b; Cugerone et al., 2021a; Cugerone et al., 2021b; Fig. 2A). Based on their close spatial and similar structural relationships with the Bentaillou deposit, we suggest

a late-Carboniferous age for D1-related stratabound Pb-Zn ores in the Bossòst Suprastructure. In the Infrastructure, Pb-Zn stratabound ores are intensely reworked at small scale by D2 deformation (i.e. saddle-reef in tight F2 folds from the Victoria deposit; Cugerone et al., 2018b). Therefore, if we consider that D2 structural reworking is late-Variscan in age, D1 structures and the associated Pb-Zn ore mineralization may be interpreted as late-Carboniferous or older.

Our geochronological data give new insights on the relationships between tectono-metamorphic events and the timing of Pb-Zn mineralization formation in the Bossòst dome (Fig. 10). During the climax of the Variscan tectonic with probable transition between MT-MP and HT-LP metamorphisms, and assuming an original Ordovician sedimentary metal stock source, we propose that pre-existing disseminated galena, sphalerite and other minor sulfides still locally preserved in surrounding metasedimentary rocks, have been intensely remobilized by the metamorphic fluids circulation leading to the formation of Pb-Zn mineralization in structural traps such as D1-structures (i.e. foliations, recumbent folds, thrusts) and/or lithological interfaces. During Variscan orogenic collapse, local remobilization of pre-existing stratabound orebodies has occured in D2-structures (i.e. fold hinges, thrusts and cleavages, Fig. 10) (Cugerone et al., 2018b; García-Sansegundo et al., 2014).

Elsewhere in the PAZ, abundant Pb-Zn ores are hosted in Ordovician metasedimentary rocks (i.e. Pierrefitte district in the Fig. 1B) and are certainly related to D1-Variscan tectonic (Cugerone et al., 2018b; Nicol et al., 1997). Furthermore, in the Basque massifs close to the PAZ (i.e. Cinco Villas in the Fig. 1B), numerous Pb-Zn ores are hosted in late-Carboniferous low-grade metasedimentary rocks and display similar structural patterns (Pesquera and Velasco, 1993; Pesquera and Velasco, 1989). Consequently, we may speculate that a regional Pb-Zn mineralization/remobilization event occurred at orogen scale, but this assumption needs to be confirmed by further direct dating of Pb-Zn ores.

Finally, metal (re)mobilization during structural inversion periods is not specific to the Bossòst Pb-Zn deposits. Structurally-controlled mineralization has already been described elsewhere in the world, like in the Australia's world class Carpentaria zinc belt (Gibson and Edwards, 2020). As an example, the Century Pb-Zn deposit is described as syn-orogenic and has formed during crustal shortening in an overall compressive tectonic regime (Polito et al., 2006). More generally, the structural and petrographical comparison between several Pb-Zn deposits of northern Australia by Perkins and Bell (1998) evidences a possible metal deposition during shortening events, as shown by structural architecture of the basins (Gibson and Edwards, 2020; Gibson et al., 2017). These structural arguments are supported by petrographic and chemical observations on Pb-Zn ores that highlight the key role of carbonate dissolution for sphalerite precipitation (Spinks et al., 2021). Similarly, at the distal edge of the Western-European Variscan orogen, structurally-controlled Pb-Zn mineralization of Carboniferous age is already known. For example, the Northern England Pb-Zn district (Aston Block) and the Irish fields have been dated by the Re-Os method on pyrite at 304 ± 20 Ma (Dempsey et al., 2021), and at 334 ± 6 Ma and 347 ± 3 Ma (Hnatyshin et al., 2015), respectively.

In the Irish ore fields, the stratabound carbonate-hosted Pb-Zn deposits of Visean age show strong spatial and genetic associations with the reactivated large-scale extensional Caledonian basement faults (Hnatyshin et al., 2015; Torremans et al., 2018; and references therein). Through 3D modeling, Torremans et al., (2018) have identified distinct points along segmented normal faults as the sources of individual deposits allowing hot, hydrothermal, metal-bearing fluids to penetrate host rocks and form these deposits. These normal fault zones developed during the lower Carbonifereous rifting event (Hitzman, 1999). Moreover, in their genetic model, based on the close relationship between Pb-Zn mineralization and extensional Carboniferous volcanic activity in the region, Wilkinson and Hitzman (2015) suggested that the key driver of fluid flow is generated by magmatic heat derived from underlying folding and mid-crustal granitic sills.

7. Conclusions

Based on a syn-mineralization U-Th-Pb monazite age (309 ± 11 Ma), we propose that stratabound Pb-Zn ore formation in the PAZ is synchronous to the main Variscan tectono-metamorphic and magmatic phase. Ore formation may be related to intense sulfide remobilization during the circulation of metamorphic fluid in an initially metal-rich crust. Our data also constrain D1 deformation to a maximum late-Carboniferous age in the Suprastructure. Monazite and zircon with Visean-Serpukhovian and Late-Carboniferous ages confirm the pre-existing data in the southern part of the Bossòst dome that recorded Variscan poly-magmatism and metamorphism. We present a new three stages geodynamic model with a crustal thickening stage related to the local formation of Visean-Serpukhovian magmatism, followed by a widespread Late-Carboniferous magmatic stage associated with a general increase of the thermal gradient, mainly in the lower crustal levels. The end of the Variscan tectono-metamorphic event is marked by leucogranite dyke intrusions and regional late-orogenic exhumation. This work shows the importance to link magmatism, metamorphism and mineralization dating to understand the geodynamic framework of ore deposit formation in orogens.

Declaration of Competing Interest

The authors declare that they have no known competing financial interests or personal relationships that could have appeared to influence the work reported in this paper.

Acknowledgments

This study was funded through the French national program "Référentiel Géologique de France" (RGF-Pyrénées) of the French Geological Survey (Bureau de Recherches Géologiques et Minières; BRGM) and through the INSU-CNRS Tellus CESSUR program. We thank Cyprien Astoury for mineral separation as well as Christophe Nevado and Doriane Delmas for thick sections preparation. We thank the ARSHAL association for Bentaillou mine access and particularly, Bernard Lafage, Louis de Pazzis and Jean-Marc Poudevigne for the extensive exploration of these Pyrenean sites and their preservation. Bénédicte Cenki acknowledges the funding from the European Union's Horizon 2020 research and innovation program under grant agreement No 793978.

Appendix A. Supplementary data

Supplementary data to this article can be found online at https://doi.org/10.1016/j.oregeorev.2021.104503.

References

Admou, S., Branquet, Y., Badra, L., Barbanson, L., Outhounjite, M., Khalifa, A., Zouhair, M., Maacha, L., 2018. The Hajjar regional transpressive shear zone (Guemassa massif, morocco): consequences on the deformation of the base-metal massive sulfide ore. Minerals 8, 1–21. https://doi.org/10.3390/min8100435.

Aguilar, C., Liesa, M., Castiñeiras, P., Navidad, M., 2014. Late Variscan metamorphic and magmatic evolution in the eastern Pyrenees revealed by U-Pb age zircon dating. J. Geol. Soc. London 171, 181–192. https://doi.org/10.1144/jgs2012-086.

Aguilar, C., Liesa, M., Štípská, P., Schulmann, K., Muñoz, J.A., Casas, J.M., 2015. P-T-t-d evolution of orogenic middle crust of the Roc de Frausa Massif (Eastern Pyrenees): a result of horizontal crustal flow and Carboniferous doming?. J. Metamorph. Geol. 33, 273–294. https://doi.org/10.1111/jmg.12120.

Alonso, J.L., 1979. Deformaciones sucesivas en el area comprendida entre Liat y el Puerto de Orla - Control estructural de los depositos de sulfuros (Valle de Aran, Pirineos Centrales). Tesis Licenciatura, Univ. Oviedo 26p.

Bois, J.P., Pouit, G., Gros, Y.B.G., Picot, P., 1976. Les minéralisations de Zn (Pb) de l'anticlinorium de Pierrefitte: un exemple de gisements hydrothermaux et sédimentaires associés au volcanisme dans le Paléozoïque des Pyrénées centrales. Bull. du BRGM 6, 543–567.

Bosse, V., Boulvais, P., Gautier, P., Tiepolo, M., Ruffet, G., Devidal, J.L., Cherneva, Z., Gerdjikov, I., Paquette, J.L., 2009. Fluid-induced disturbance of the monazite Th-Pb chronometer: in situ dating and element mapping in pegmatites from the Rhodope (Greece, Bulgaria). Chem. Geol. 261, 286–302. https://doi.org/10.1016/

j.chemgeo.2008.10.025.
Boutin, A., de Saint Blanquat, M., Poujol, M., Boulvais, P., de Parseval, P., Rouleau, C., Robert, J.F., 2016. Succession of Permian and Mesozoic metasomatic events in the eastern Pyrenees with emphasis on the Trimouns talc–chlorite deposit. Int. J. Earth Sci. 105, 747–770. https://doi.org/10.1007/s00531-015-1223-x.
Burisch, M., Gerdes, A., Meinert, L.D., Albert, R., Seifert, T., Gutzmer, J., 2019. The essence of time – fertile skarn formation in the Variscan Orogenic Belt. Earth Planet. Sci. Lett. 519, 165–170. https://doi.org/10.1016/j.epsl.2019.05.015.
Cardellach, E., Canals, A., Pujals, I., 1996. La composicion isotopica del azufre y del plomo en las mineralizaciones de Zn-Pb del Valle de Aran (Pirineo Central) y su significado metalogenetico. Estud. Geol. 52, 189–195.
Carreras, J., Capella, I., 1994. Tectonic levels in the Palaeozoic basement of the Pyrenees: a review and a new interpretation. J. Struct. Geol. 16, 1509–1524.
Carreras, J., Cirés, J., 1986. The geological significance of the western termination of the Mérens Fault at Port Vell (central Pyrenees). Tectonophysics 129, 99–114. https://doi.org/10.1016/0040-1951(86)90248-9.
Carreras, J., Druguet, E., 2014. Framing the tectonic regime of the NE Iberian Variscan segment. Schulmann, K., al., eds., Variscan Orogeny Extent, Timescale Form. Eur. Crust Geol. Soc. London, Spec. Publ. 405, 249–264. https://doi.org/10.1144/SP405.7.
Carreras, J., Druguet, E., Griera, A., Soldevila, J., 2004. Strain and deformation history in a syntectonic pluton. The case of the Roses granodiorite (Cap de Creus, Eastern Pyrenees). Geol. Soc. London Spec. Publ. 224, 307–319. https://doi.org/10.1144/GSL.SP.2004.224.01.19.
Carreras, J., Julivert, M., Santanach, P., 1980. Hercynian mylonite belts in the eastern Pyrenees: an example of shear zones associated with late folding. J. Struct. Geol. 2, 5–9. https://doi.org/10.1016/0191-8141(80)90028-0.
Castroviejo Bolibar, R., Serrano, F.M., 1983. Estructura y metalogenia del campo filoniano de Cierco (Pb-Zn-Ag), en el Pirineo de Lérida. Boletín Geológio y Min. 1983, 291–320.
Cave, B., Lilly, R., Barovich, K., 2020. Textural and geochemical analysis of chalcopyrite, galena and sphalerite across the Mount Isa Cu to Pb-Zn transition: implications for a zoned Cu-Pb-Zn system. Ore Geol. Rev. 124, 103647. https://doi.org/10.1016/j.oregeorev.2020.103647.
Chauvet, A., Onézime, J., Charvet, J., Barbanson, L., Faure, M., 2004. Syn to late tectonic stockwork emplacement within the Spanish section of the Iberian Pyrite Belt: structural, textural, and mineralogical constraints in the Tharsis and La Zarza areas. Econ. Geol. 99, 1781–1792. https://doi.org/10.1055/s-2002-30668.
Cherniak, D.J., Watson, E.B., Grove, M., Harrison, T.M., 2004. Pb diffusion in monazite: a combined RBS/SIMS study. Geochim. Cosmochim. Acta 68, 829–840. https://doi.org/10.1016/j.gca.2003.07.012.
Choukroune, P., 1992. Tectonic evolution of the Pyrenees. Annu. Rev. Earth Planet. Sci. 20, 143–158.
Cochelin, B., 2016. Champ de déformation du socle Paléozoïque des Pyrénées. PhD Thesis. Université Toulouse 3 Paul Sabatier.
Cochelin, B., Chardon, D., Denèle, Y., Gumiaux, C., Le Bayon, B., 2017a. Vertical strain partitioning in hot Variscan crust: syn-convergence escape of the Pyrenees in the Iberian-Armorican syntax. Bull. la Société géologique Fr. 188, 39. https://doi.org/10.1051/bsgf/2017206.
Cochelin, B., Lemirre, B., Denèle, Y., De Saint Blanquat, M., Lahfid, A., Duchêne, S., 2017b. Structural inheritance in the Central Pyrenees : the Variscan to Alpine tectonometamorphic evolution of the Axial Zone. J. Geol. Soc. London 175, 336–351. https://doi.org/10.1144/jgs2017-066.
Cocherie, A., Baudin, T., Autran, A., Guerrot, C., Fanning, C.M., Laumonier, B., 2005. U-Pb zircon (ID-TIMS and SHRIMP) evidence for the early ordovician intrusion of metagranites in the Late Proterozoic Canaveilles Group of the Pyrenees and the Montagne Noire (France). Bull. la Soc. Geol. Fr. 176, 269–282. https://doi.org/10.2113/176.3.269.
Cugerone, A., Cenki-Tok, B., Chauvet, A., Le Goff, E., Bailly, L., Alard, O., Allard, M., 2018a. Relationships between the occurrence of accessory Ge-minerals and sphalerite in Variscan Pb-Zn deposits of the Bossost anticlinorium, French Pyrenean Axial Zone: chemistry, microstructures and ore-deposit setting. Ore Geol. Rev. 95, 1–19. https://doi.org/10.1016/j.oregeorev.2018.02.016.
Cugerone, A., Cenki-tok, B., Muñoz, M., Kouzmanov, K., Oliot, E., Motto-ros, V., Goff, E.L., Motto-ros, V., 2021a. Behavior of critical metals in metamorphosed Pb-Zn ore deposits: example from the Pyrenean Axial Zone. Miner. Depos. 56, 685–705. https://doi.org/10.1007/s00126-020-01000-9.
Cugerone, A., Cenki-tok, B., Oliot, E., Muñoz, M., Barou, F., Motto-Ros, V., Le Goff, E., 2020. Redistribution of germanium during dynamic recrystallization of sphalerite. Geology 48, 236–241. https://doi.org/10.1130/G46791.1.
Cugerone, A., Cenki, B., Oliot, E., Muñoz, M., 2021b. Structure and Texture of Pb-Zn Mineralization: Example of a Multiscale Study in the Pyrenees to Constrain Ore-forming Processes and Critical Metals Mobility. ISTE-WILEY-Science Encycl. - Rev..
Cugerone, A., Oliot, E., Chauvet, A., Gavaldà Bordes, J., Laurent, A., Le Goff, E., Cenki-Tok, B., 2018b. Structural control on the formation of Pb-Zn deposits: an example from the pyrenean axial zone. Minerals 8, 1–20. https://doi.org/10.3390/min8110489.
Cumming, G.L., Richards, J.R., 1975. Ore lead isotope ratios in a continuously changing earth. Earth Planet. Sci. Lett. 28, 155–171. https://doi.org/10.1016/0012-821X(75)90223-X.
de Hoÿm de Marien, L., Le Bayon, B., Pitra, P., Van Den Driessche, J., Poujol, M., Cagnard, F., 2019. Two-stage Variscan metamorphism in the Canigou massif: evidence for crustal thickening in the Pyrenees. J. Metamorph. Geol. 1–26. https://doi.org/10.1111/jmg.12487.
De Sitter, L.U., Zwart, H.J., 1960. Tectonic development in supra and infra-structures of a mountain chain. In: Proc. 21st Int Geol. Congr. Copenhagen. pp. 248–256.
Debon, F., 1980. Genesis of the three concentrically-zoned granitoid Plutons of Cauterets-Panticosa (French and Spanish Western Pyrenees). Geol. Rundschau 69, 107–130. https://doi.org/10.1007/BF01869027.
Deloule, E., Alexandrov, P., Cheilletz, A., Laumonier, B., Barbey, P., 2002. In-situ U-Pb zircon ages for Early Ordovician magmatism in the eastern Pyrenees, France: the Canigou orthogneisses. Int. J. Earth Sci. 91, 398–405. https://doi.org/10.1007/s00531-001-0232-0.
Delvolvé, J.J., Souquet, P., Vachard, D., Perret, M.F., Aguirre, P., 1993. Caractérisation d'un bassin d'avant-pays dans le Carbonifère des Pyrénées: faciès, chronologie de la tectonique synsédimentaire. C. R. Acad. Sci. Paris 316, 959–966.
Delvolvé, J.J., Vachard, D., Souquet, P., 1998. Stratigraphic record of thrust propagation, Carboniferous foreland basin, Pyrenees, with emphasis on Pays-de-Sault (France/Spain). Int. J. Earth Sci. 87, 363–372.
Dempsey, E.D., Holdsworth, R.E., Selby, D., Bird, A., Young, B., Le Cornu, C., 2021. A revised age, structural model and origin for the North Pennine Orefield in the Alston Block, northern England: intrusion (Whin Sill)-related base metal (Cu–Pb–Zn–F) mineralization. J. Geol. Soc. London 178. jgs2020-226. https://doi.org/10.1144/jgs2020-226.
Denèle, Y., Laumonier, B., Paquette, J.-L., Olivier, P., Gleizes, G., Barbey, P., 2014. Timing of granite emplacement, crustal flow and gneiss dome formation in the Variscan segment of the Pyrenees. Schulmann, K., al., eds., Variscan Orogeny Extent, Timescale Form. Eur. Crust Geol. Soc. London, Spec. Publ. 405, 265–287. https://doi.org/10.1144/SP405.5.
Denèle, Y., Olivier, P., Gleizes, G., 2008. Progressive deformation of a zone of magma transfer in a transpressional regime: the Variscan Mérens shear zone (Pyrenees, France). J. Struct. Geol. 30, 1138–1149. https://doi.org/10.1016/j.jsg.2008.05.006.
Denèle, Y., Olivier, P., Gleizes, G., Barbey, P., 2007. The Hospitalet gneiss dome (Pyrenees) revisited: Lateral flow during Variscan transpression in the middle crust. Terra Nov. 19, 445–453. https://doi.org/10.1111/j.1365-3121.2007.00770.x.
Denèle, Y., Paquette, J.L., Olivier, P., Barbey, P., 2012. Permian granites in the Pyrenees: the Aya pluton (Basque Country). Terra Nov. 24, 105–113. https://doi.org/10.1111/j.1365-3121.2011.01043.x.
Didier, A., Bosse, V., Cherneva, Z., Gautier, P., Georgieva, M., Paquette, J.L., Gerdjikov, I., 2014. Syn-deformation fluid-assisted growth of monazite during renewed high-grade metamorphism in metapelites of the Central Rhodope (Bulgaria, Greece). Chem. Geol. 381, 206–222. https://doi.org/10.1016/j.chemgeo.2014.05.020.
Druguet, E., Castro, A., Chichorros, M., Pereira, M.F., Fernandez, C., 2014. Zircon geochronology of intrusive rocks from Cap de Creus, Eastern Pyrenees. Geol. Mag. 151, 1095–1114. https://doi.org/10.1017/S0016756814000041.
Essaifi, A., Goodenough, K., Tornos, F., Outigua, A., Ouadjou, A., Maacha, L., 2019. The Moroccan Massive Sulphide Deposits: evidence for a Polyphase Mineralization. Minerals 9, 1–31. https://doi.org/10.3390/min9030156.
Esteban, J.J., Aranguren, A., Cuevas, J., Hilario, A., Tubía, J.M., Larionov, A., Sergeev, S., 2015. Is there a time lag between the metamorphism and emplacement of plutons in the Axial Zone of the Pyrenees?. Geol. Mag. 1–7. https://doi.org/10.1017/S001675681500014X.
Evans, N.G., Gleizes, G., Leblanc, D., Bouchez, J.L., 1998. Syntectonic emplacement of the Maladeta granite (Pyrenees) deduced from relationships between Hercynian deformation and contact metamorphism. J. Geol. Soc. London 155, 209–216. https://doi.org/10.1144/gsjgs.155.1.0209.
Fallourd, S., Poujol, M., Boulvais, P., Paquette, J.L., de Saint Blanquat, M., Rémy, P., 2014. In situ LA-ICP-MS U-Pb titanite dating of Na-Ca metasomatism in orogenic belts: the North Pyrenean example. Int. J. Earth Sci. 103, 667–682. https://doi.org/10.1007/s00531-013-0978-1.
Fert, D., 1976. Un aspect de la métallogénie du zinc et du plomb dans l'Ordovicien des Pyrénées Centrales: le district de Sentein (Ariège, Haute-Garonne). Ph.D Thesis. Univ Pierre Marie Curie, p. 149.
Frenzel, M., Hirsch, T., Gutzmer, J., 2016. Gallium, germanium, indium, and other trace and minor elements in sphalerite as a function of deposit type - a meta-analysis. Ore Geol. Rev. 76, 52–78. https://doi.org/10.1016/j.oregeorev.2015.12.017.
García-Sansegundo, J., 1996. Hercynian structure of the Axial Zone of the Pyrenees: the Aran Valley cross-section (Spain-France). J. Struct. Geol. 18, 1315–1325. https://doi.org/10.1016/S0191-8141(96)00050-8.
García-Sansegundo, J., Alonso, J.L., 1989. Stratigraphy and structure of the southeastern Garona Dome. Geodin. Acta 3, 127–134. https://doi.org/10.1080/09853111.1989.11105180.
García-Sansegundo, J., Martin-Izard, A., Gavaldà, J., 2014. Structural control and geological significance of the Zn-Pb ores formed in the Benasque Pass area (Central Pyrenees) during the post-late Ordovician extensional event of the Gondwana margin. Ore Geol. Rev. 56, 516–527. https://doi.org/10.1016/j.oregeorev.2013.06.001.
García-Sansegundo, J., Poblet, J., Alonso, J.L., Clariana, P., 2011. Hinterland-foreland zonation of the Variscan Orogen in the central Pyrenees: Comparison with the northern part of the Iberian Variscan Massif. Geol. Soc. Spec. Publ. 349, 169–184. https://doi.org/10.1144/SP349.9.
Gardés, E., Montel, J.M., Seydoux-Guillaume, A.M., Wirth, R., 2007. Pb diffusion in monazite: new constraints from the experimental study of Pb2 + ⇔ Ca2 + interdiffusion. Geochim. Cosmochim. Acta 71, 4036–4043. https://doi.org/10.1016/j.gca.2007.06.036.
Gibson, G., Edwards, S., 2020. Basin inversion and structural architecture as constraints on fluid flow and Pb-Zn mineralisation in the Paleo-Mesoproterozoic sedimentary sequences of northern Australia. Solid Earth Discuss. 1–26. https://doi.org/10.5194/se-2020-31.
Gibson, G.M., Hutton, L.J., Holzschuh, J., 2017. Basin inversion and supercontinent assembly as drivers of sediment-hosted Pb–Zn mineralization in the Mount Isa region, northern Australia. J. Geol. Soc. London 174. jgs2016-105. https://doi.org/10.1144/jgs2016-105.
Gigon, J., Deloule, E., Mercadier, J., Huston, D.L., Richard, A., Annesley, I.R., Wygralak, A.S., Skirrow, R.G., Mernagh, T.P., Masterman, K., 2020. Tracing metal sources for the giant McArthur River Zn-Pb deposit (Australia) using lead isotopes. Geology 48, 478–482. https://doi.org/10.1130/G47001.1.

Gleizes, G., Crevon, G., Asrat, A., Barbey, P., 2006. Structure, age and mode of emplacement of the Hercynian Bordères-Louron pluton (Central Pyrenees, France). Int. J. Earth Sci. 95, 1039–1052. https://doi.org/10.1007/s00531-006-0088-4.
Guitard, G., Geyssant, J., Laumonier, B., 1984. Les plissements hercyniens tardifs dans le Paléozoïque inférieur du versant nord du Canigou. 1re partie: analyse géométrique et chronologie des phases superposees. Relations avec le granite de Mont-Louis et le métamorphisme régional. Géologie la Fr. 4, 95–125.
Hetherington, C.J., Harlov, D.E., Budzyń, B., 2010. Experimental metasomatism of monazite and xenotime: mineral stability, REE mobility and fluid composition. Mineral. Petrol. 99, 165–184. https://doi.org/10.1007/s00710-010-0110-1.
Hitzman, M.W., 1999. Extensional faults that localize Irish syndiagenetic Zn-Pb Deposits and their reactivation during Variscan compression. Geol. Soc. Spec. Publ. 155, 233–245. https://doi.org/10.1144/GSL.SP.1999.155.01.17.
Hnatyshin, D., Creaser, R.A., Wilkinson, J.J., Gleeson, S.A., 2015. Re-Os dating of pyrite confirms an early diagenetic onset and extended duration of mineralization in the Irish Zn-Pb ore field. Geology 43, 143–146. https://doi.org/10.1130/G36296.1.
Hurai, V., Paquette, J.-L., Huraiová, M., Konečný, P., 2010. Age of deep crustal magmatic chambers in the intra-Carpathian back-arc basin inferred from LA-ICPMS U-Th-Pb dating of zircon and monazite from igneous xenoliths in alkali basalts. J. Volcanol. Geoth. Res. 198, 275–287.
Jackson, S.E., Pearson, N.J., Griffin, W.L., Belousova, E.A., 2004. The application of laser ablation-inductively coupled plasma-mass spectrometry to in situ U-Pb zircon geochronology. Chem. Geol. 211, 47–69. https://doi.org/10.1016/j.chemgeo.2004.06.017.
Jaffey, A.H., Flynn, K.F., Glendenin, L.E., Bentley, W.C., Essling, A.M., 1971. Precision measurement of half-lives and specific activities of U235 and U238. Phys. Rev. C 4, 1889–1906. https://doi.org/10.1103/PhysRevC.4.1889.
Jiang, W.C., Li, H., Turner, S., Zhu, D.P., Wang, C., 2020. Timing and origin of multi-stage magmatism and related W-Mo–Pb–Zn–Fe–Cu mineralization in the Huangshaping deposit, South China: an integrated zircon study. Chem. Geol. 552, 119782. https://doi.org/10.1016/j.chemgeo.2020.119782.
Kelly, N.M., Harley, S.L., Möller, A., 2012. Complexity in the behavior and recrystallization of monazite during high-T metamorphism and fluid infiltration. Chem. Geol. 322–323, 192–208. https://doi.org/10.1016/j.chemgeo.2012.07.001.
Kelly, W.C., Clark, B.R., 1975. Sulfide deformation studies: III. experimental deformation of chalcopyrite to 2,000 bars and 500??C. Econ. Geol. 70, 431–453. https://doi.org/10.2113/gsecongeo.70.3.431.
Kilzi, M.A., Grégoire, M., Bosse, V., Benoît, M., Driouch, Y., de Saint Blanquat, M., Debat, P., 2016. Geochemistry and zircon U-Pb geochronology of the ultramafic and mafic rocks emplaced within the anatectic series of the Variscan Pyrenees: the example of the Gavarnie-Heas dome (France). C. R. - Geosci. 348, 107–115. https://doi.org/10.1016/j.crte.2015.06.014.
Kleinsmiede, W.F.J., 1960. Geology of the Valle de Aran (Central Pyrenees), Leidse. Geol. Meded. 25, 129–245.
Kollenberg, W., Siemes, H., 1983. Experimental deformation of sphalerite-garnet ore under a confining pressure of 300 MPa and at temperature between 25°C and 300°C. Bild. J.B., al., eds., Deform. Multi-Phase Part. Contain. Mater. Roskilde, Denmark, Risø Natl. Lab. pp. 351–356.
Laumonier, B., Autran, A., Barbey, P., Cheilletz, A., Baudin, T., Cocherie, A., Guerrot, C., 2004. Conséquences de l'absence de socle cadomien sur l'âge et la signification des séries pré-varisques (anté-Ordovicien supérieur) du sud de la France (Pyrénées, Montagne Noire). Bull. la Société Geol. Fr. 175, 643–655.
Laumonier, B., Calvet, M., Barbey, P., Guennoc, P., Lambert, J., Wiazemsky, M., 2013. Notice explicative, Carte géologique de France (1/50 000), feuille Argelès-sur-Mer-Cerbère (1097). Cart. géologique par Calvet M., Autran A., Wiaz. M., Laumonier B., Guitar. G.† (2015). Orléans BRGM 149p.
Laumonier, B., Le Bayon, B., Calvet, M., 2015. Carte géol. France (1/50 000), feuille Prats-de-Mollo-la-Preste (1099). BRGM Not. Explic. par Laumonier B., Calvet M., Le Bayon B., Barbey P., Lenoble J.-L. 189p.
Laumonier, B., Marignac, C., Kister, P., 2010. Polymétamorphisme et évolution crustale dans les Pyrénées orientales pendant l'orogenèse varisque au Carbonifère supérieur. Bull. la Société géologique Fr. 181, 411–428.
Laurent, O., Couzinié, S., Zeh, A., Vanderhaeghe, O., Moyen, J.F., Villaros, A., Gardien, V., Chelle-Michou, C., 2017. Protracted, coeval crust and mantle melting during Variscan late-orogenic evolution: U-Pb dating in the eastern French Massif Central. Int. J. Earth Sci. 106, 421–451. https://doi.org/10.1007/s00531-016-1434-9.
Le Bayon, B., Cochelin, B., 2020. Anatomy of an extensional shear zone leading to the exhumation of the middle crust within the Canigou dome (Eastern Pyrenees, Axial Zone). J. Struct. Geol. 183135. https://doi.org/10.1016/j.jsg.2020.104200.
Lemirre, B., 2018. Origine et développement de la thermicité dans les Pyrénées Varisques. Ph.D Thesis. Univ Toulouse III, pp. 1–289.
Lemirre, B., Cochelin, B., Duchene, S., de Saint Blanquat, M., Poujol, M., 2019. Origin and duration of late orogenic magmatism in the foreland of the Variscan belt (Lesponne — Chiroulet — Neouvielle area, French Pyrenees). Lithos 336–337, 183–201. https://doi.org/10.1016/j.lithos.2019.03.037.
Lopez-Sanchez, M.A., Aleinikoff, J.N., Marcos, A., Martínez, F.J., Llana-Fúnez, S., 2016. An example of low-Th/U zircon overgrowths of magmatic origin in a late orogenic variscan intrusion: the San Ciprián massif (NW Spain). J. Geol. Soc. London 173, 282–291. https://doi.org/10.1144/jgs2015-071.
Lopez-Sanchez, M.A., García-Sansegundo, J., Martínez, F.J., 2019. The significance of early Permian and early Carboniferous U-Pb zircon ages in the Bossòst and Lys-Caillaouas granitoids (Pyrenean Axial Zone). Geol. J. 1–16. https://doi.org/10.1002/gj.3283.
Ludwig, K.R., 2001. User's manual for Isoplot/Ex Version 2.49, a geochronological toolkit for Microsoft Excel. Berkeley Geochronological Center, Spec. Publ. 1a, Berkeley, USA, 55p.
Marcoux, E., 1986. Isotope du plomb et paragénèses métalliques, traceurs de l'histoire des gites mineraux. Bur. Rech. Geol. Minière.
Marcoux, E., Joubert, M., Lescuyer, J.L., 1991. Origine des mineralisations stratiformes de la bordere du Canigou (Pyrenees orientales, France): apport de la geochimie isotopique du plomb. Compte Rendu Acad. Sci. Paris II 312,II,281, 281–287.
Marignac, C., Diagana, B., Cathelineau, M., Boiron, M.C., Banks, D., Fourcade, S., Vallance, J., 2003. Remobilisation of base metals and gold by Variscan metamorphic fluids in the south Iberian pyrite belt: evidence from the Tharsis VMS deposit. Chem. Geol. 194, 143–165. https://doi.org/10.1016/S0009-2541(02)00275-9.
Martín-Closas, C., Trias, S., Casas, J.M., 2018. New palaeobotanical data from carboniferous culm deposits constrain the age of the variscan deformation in the eastern pyrenees. Geol. Acta 16, 107–123. https://doi.org/10.1344/GeologicaActa2018.16.2.1.
Martinez Catalan, J.R., 2011. Are the oroclines of the Variscan belt related to late Variscan strike-slip tectonics?. Terra Nov. 23, 241–247. https://doi.org/10.1111/j.1365-3121.2011.01005.x.
Martínez, F.J., Dietsch, C., Aleinikoff, J., Cirés, J., Arboleya, M.L., Reche, J., Gómez-Gras, D., 2016. Provenance, age, and tectonic evolution of Variscan flysch, southeastern France and northeastern Spain, based on zircon geochronology. Geol. Soc. Am. Bull. 128, 842–859. https://doi.org/10.1130/b31316.1.
Martínez, F.J., Reche, J., Iriondo, A., 2008. U-Pb Shrimp-RG zircon ages of Variscan igneous rocks from the Guilleries massif (NE Iberia pre-Mesozoic basement), Geological implications. C. R. - Geosci. 340, 223–232. https://doi.org/10.1016/j.crte.2007.12.006.
Matte, P., 2002. Les plis hercyniens kilométriques couchés vers l'ouest-sud-ouest dans la région du pic du Midi d'Ossau-col du Somport (zone axiale des Pyrénées occidentales). C. R. - Geosci. 334, 773–779. https://doi.org/10.1016/S1631-0713(02)01808-4.
Matte, P., 2001. The Variscan collage and orogeny (480–290 Ma) and the tectonic definition of the Armorica microplate: a review. Terra Nov. 13, 122–128.
Matte, P., 1969. Le problème du passage de la schistosité horizontale à la schistosité verticale dans le dôme de la Garonne (Paléozoïque des Pyrénées Centrales). Compte Rendu Acad. Sci. Paris II 268, Série D-1841-1844.
Maurel, O., 2003. L'exhumation de la Zone Axiale des Pyrénées orientales : Une approche thermo-chronologique multi-méthodes du rôle des failles.
Maurel, O., Respaut, J.P., Monié, P., Arnaud, N., Brunel, M., 2004. U-Pb emplacement and 40Ar/39Ar cooling ages of the eastern Mont-Louis granite massif (Eastern Pyrenees, France). C. R. - Geosci. 336, 1091–1098. https://doi.org/10.1016/j.crte.2004.04.005.
Mezger, J.E., 2005. Comparison of the western Aston-Hospitalet and the Bossòst domes: evidence for polymetamorphism and its implications for the Variscan tectonic evolution of the Axial Zone of the Pyrenees. J. Virtual Explor. 19, 1–19. https://doi.org/10.3809/jvirtex.2005.00122.
Mezger, J.E., Gerdes, A., 2016. Early Variscan (Visean) granites in the core of central Pyrenean gneiss domes: implications from laser ablation U-Pb and Th-Pb studies. Gondwana Res. 29, 181–198. https://doi.org/10.1016/j.gr.2014.11.010.
Mezger, J.E., Passchier, C.W., 2003. Polymetamorphism and ductile deformation of staurolite–cordierite schist of the Bossòst dome: indication for Variscan extension in the Axial Zone of the central Pyrenees. Geol. Mag. 140, 595–612. https://doi.org/10.1017/S0016756803008112.
Mezger, J.E., Passchier, C.W., Régnier, J.-L., 2004. Metastable staurolite–cordierite assemblage of the Bossòst dome: late Variscan decompression and polyphase metamorphism in the Axial Zone of the central Pyrenees. C. R. Geosci. 336, 827–837. https://doi.org/10.1016/j.crte.2003.12.024.
Mezger, J.E., Régnier, J.L., 2016. Stable staurolite-cordierite assemblages in K-poor metapelitic schists in Aston and Hospitalet gneiss domes of the central Pyrenees (France, Andorra). J. Metamorph. Geol. 34, 167–190. https://doi.org/10.1111/jmg.12177.
Mezger, J.E., Schnapperelle, S., Rölke, C., 2012. Evolution of the Central Pyrenean Mérens fault controlled by near collision of two gneiss domes. Jahrb. für Geowissenschaften 34, 11–29.
Milodowski, A.E., Zalasiewicz, J.A., 1991. Redistribution of rare earth elements during diagenesis of turbidite/hemipelagite mudrock sequences of Llandovery age from central Wales. Geol. Soc. Spec. Publ. 57, 101–124. https://doi.org/10.1144/GSL.SP.1991.057.01.10.
Munoz, M., Baron, S., Boucher, A., Béziat, D., Salvi, S., 2016. Mesozoic vein-type Pb–Zn mineralization in the Pyrenees: lead isotopic and fluid inclusion evidence from the Les Argentières and Lacore deposits. C. R. Geosci. 348, 322–332. https://doi.org/10.1016/j.crte.2015.07.001.
Murphy, T.E., 2004. Structural and stratigraphic controls on mineralization at the George Fisher Zn-Pb-Ag Deposit, northwest Queensland, Australia. Ph. D Thesis. James Cook Univ., pp. 1–423.
Nicol, N., Legendre, O., Charvet, J., 1997. Les minéralisations Zn-Pb de la série paléozoïque de Pierrefitte (Hautes-Pyrénées) dans la succession des évènements tectoniques hercyniens. C.R Acad. Sci. Paris 324, 453–460.
Ostkamp, M., Schnapperelle, S., Mertmann, D., 2019. Strukturgeologische Charakterisierung der Mérens Scher-und Störungszone bei Mérens-les-Vals (französische Pyrenäen). Hallesches Jahrb. für Geowissenschaften 42, 69–111.
Paquette, J.L., Gleizes, G., Leblanc, D., Bouchez, J.L., 1997. Le granite de Bassies (Pyrénées): un pluton syntectonique d'âge westphalien. Géochronologie U– Pb sur zircons. C. R. Acad. Sci. Paris 324, 387–392.
Paquette, J.L., Piro, J.L., Devidal, J.L., Bosse, V., Didier, A., 2014. Sensitivity enhancement in LA-ICP-MS by N2 addition to carrier gas: application to radiometric dating of U-Th- bearing minerals. Agil. ICP-MS J. 58, 4–5.
Pereira, M.F., Castro, A., Chichorro, M., Fernández, C., Díaz-Alvarado, J., Martí, J., Rodríguez, C., 2014. Chronological link between deep-seated processes in magma chambers and eruptions: Permo-Carboniferous magmatism in the core of Pangaea (Southern Pyrenees). Gondwana Res. 25, 290–308. https://doi.org/10.1016/j.gr.2013.03.009.
Perkins, W.G., Bell, T.H., 1998. Stratiform replacement lead-zinc deposits: a comparison between Mount Isa, Hilton, and McArthur River. Econ. Geol. 93, 1190–1212. https://

doi.org/10.2113/gsecongeo.93.8.1190.
Pesquera, A., Velasco, F., 1993. Ore Metamorphism in Sulfide Mineralizations from the Cinco Villas Massif (Western Pyrenees, Spain). Econ. Geol. 88, 266–282.
Pesquera, A., Velasco, F., 1989. The arditurri Pb-Zn-F-Ba deposit (Cinco Villas massif, Basque Pyrenees): a deformed and metamorphosed stratiform deposit. Miner. Depos. 24, 199–209. https://doi.org/10.1007/BF00206443.
Poitrenaud, T., Poujol, M., Augier, R., Marcoux, E., 2019. The polyphase evolution of a late Variscan W/Au deposit (Salau, French Pyrenees): insights from REE and U/Pb LA-ICP-MS analyses. Miner. Depos. 1–21. https://doi.org/10.1007/s00126-019-00923-2.
Polito, P.A., Kyser, T.K., Golding, S.D., Southgate, P.N., 2006. Zinc deposits and related mineralization of the Burketown mineral field, including the world-class century deposit, northern Australia: fluid inclusion and stable isotope evidence for basin fluid sources. Econ. Geol. 101, 1251–1273. https://doi.org/10.2113/gsecongeo.101.6.1251.
Pouget, P., 1991. Hercynian Tectonometamorphic Evolution of the Bosost Dome (French Spanish Central Pyrenees). J. Geol. Soc. London 148, 299–314. https://doi.org/10.1144/gsjgs.148.2.0299.
Pouit, G., 1986. Les minéralisations Zn-Pb exhalatives sédimentaires de Bentaillou et de l 'anticlinorium paléozoïque de Bosost (Pyrénées ariégeoises, France). Chron. la Rech. minière 485, 3–16.
Pouit, G., 1985. Les minéralisations Zn (Pb) Ba du Paléozoïque des Pyrénées Centrales: Une mise au point et un compte rendu des missions 1984. Bur. Rech. Géologiques Minières Rapp. 85 (DAM037), 72.
Pouit, G., 1978. Différents Modeles de Mineralisations «Hydrothermale Sédimentaire », à Zn (Pb) du Paléozoïque des Pyrénees Centrales. Miner. Depos. 13, 411–421.
Pouit, G., Bois, J.P., 1986. Arrens Zn (Pb), Ba Devonian deposit, Pyrénées, France: an exhalative-sedimentary-type deposit similar to Meggen. Miner. Depos. 21, 181–189.
Poujol, M., Boulvais, P., Kosler, J., 2010. Regional-scale Cretaceous albitization in the Pyrenees: evidence from in situ U-Th-Pb dating of monazite, titanite and zircon. J. Geol. Soc. London 167, 751–767. https://doi.org/10.1144/0016-76492009-144.
Pujals, I., 1992. Las mineralizaciones de sulfuros en el Cambro-Ordovicico de la Val d'Aran (Pirineo Central, Lérida). Ph.D Thesis. Univ Autónoma Barcelona, p. 294.
Rasmussen, B., Fletcher, I.R., McNaughton, N.J., 2001. Dating low-grade metamorphic events by SHRIMP U-Pb analysis of monazite in shales. Geology 29, 963–966. https://doi.org/10.1130/0091-7613(2001)029<0963:DLGMEB>2.0.CO;2.
Rasmussen, B., Muhling, J.R., 2007. Monazite begets monazite: evidence for dissolution of detrital monazite and reprecipitation of syntectonic monazite during low-grade regional metamorphism. Contrib. to Mineral. Petrol. 154, 675–689. https://doi.org/10.1007/s00410-007-0216-6.
Reyx, J., 1973. Relations entre tectonique, métamorphisme de contact et concentrations metalliques dans le secteur des anciennes mines d'Arre et Anglas (Hautes-Pyrénées - Pyrénées atlantiques). Ph. D Thesis. Univ. Paris VI, p. 83.
Roberts, M.P., Pin, C., Clemens, J.D., Paquette, J.L., 2000. Petrogenesis of Mafic to Felsic Plutonic Rock Associations: the Calc-alkaline Querigut Complex, French Pyrenees. J. Petrol. 41, 809–844. https://doi.org/10.1093/petrology/41.6.809.
Romer, R.L., Soler, A., 1995. U-Pb age and lead isotopic characterization of Au-bearing skarn related to the Andorra granite (central Pyrenees, Spain). Miner. Depos. 30, 374–383. https://doi.org/10.1007/BF00202280.
Schnapperelle, S., Mezger, J.E., Stipp, M., Hofmann, M., Gärtner, A., Linnemann, U., 2020. Polyphase magmatic pulses along the Northern Gondwana margin: U-Pb zircon geochronology from gneiss domes of the Pyrenees. Gondwana Res. 81, 291–311. https://doi.org/10.1016/j.gr.2019.11.013.
Seydoux-Guillaume, A.M., Paquette, J.L., Wiedenbeck, M., Montel, J.M., Heinrich, W., 2002. Experimental resetting of the U-Th-Pb systems in monazite. Chem. Geol. 191, 165–181. https://doi.org/10.1016/S0009-2541(02)00155-9.
Siemes, H., Hennig-Michaeli, C., 1985. Ore Minerals. In: Wenk, H.R. (Ed.), Prefer. Orientat. Deform. Met. rocks, an Introd. to Mod. texture Anal.. Acad. Press, Orlando, pp. 335–360.
Siemes, H., Hennig-Michaeli, C., Martens, L., 1991. The importance of deformation experiments on minerals for the interpretation of metamorphic ore textures. Ore Geol. Rev. 6, 475–483. https://doi.org/10.1016/0169-1368(91)90042-6.
Soula, J.C., 1982. Characteristics and mode of emplacement of gniess domes and plutonic domes in central-eastern Pyrenees. J. Struct. Geol. 4, 313–337. https://doi.org/10.1016/0191-8141(82)90017-7.
Soula, J.C., Debat, P., Deramond, J., Pouget, P., 1986. The Geological Evolution of the Pyrenees A dynamic model of the structural evolution of the Hercynian Pyrenees. Tectonophysics 129, 29–51. https://doi.org/10.1016/0040-1951(86)90244-1.
Spinks, S.C., Pearce, M.A., Liu, W., Kunzmann, M., Ryan, C.G., Moorhead, G.F., Kirkham, R., Blaikie, T., Sheldon, H.A., Schaubs, P.M., Rickard, W.D.A., 2021. Carbonate replacement as the principal ore formation process in the proterozoic McArthur River (HYC) sediment-hosted Zn-Pb Deposit. Australia. Econ. Geol. 116, 693–718. https://doi.org/10.5382/econgeo.4793.
Stacey, J.S., Kramers, J.D., 1975. Approximation of terrestrial lead isotope evolution by a two-stage model. Earth Planet. Sci. Lett. 26, 207–221. https://doi.org/10.1016/0012-821X(75)90088-6.
Stampfli, G.M., Hochard, C., Vérard, C., Wilhem, C., vonRaumer, J., 2013. The formation of Pangea. Tectonophysics 593, 1–19. https://doi.org/10.1016/j.tecto.2013.02.037.
Steiger, R.H., Jäger, E., 1977. Submission on Geochronology: Convention on the use of decay constants in geo- and cosmochronology. Earth Planet. Sci. Lett. 36, 359–362.
Tartèse, R., Ruffet, G., Poujol, M., Boulvais, P., Ireland, T.R., 2011. Simultaneous resetting of the muscovite K-Ar and monazite U-Pb geochronometers: a story of fluids. Terra Nov. 23, 390–398. https://doi.org/10.1111/j.1365-3121.2011.01024.x.
Ternet, Y., Majesté-Menjoulas, C., Canérot, J., Baudin, T., Cocherie, A., Guerrot, C., Rossi, P., 2004. Carte géologique de la France - 1/50 000. Feuille 1069, Laruns-Somport. Ed. du BRGM Serv. géologique Natl. 1–195.
Tornos, F., Solomon, M., Conde, C., Spiro, B.F., 2008. Formation of the tharsis massive sulfide deposit, Iberian Pyrite Belt: Geological, lithogeochemical, and stable Isotope evidence for deposition in a brine pool. Econ. Geol. 103, 185–214. https://doi.org/10.2113/gsecongeo.103.1.185.
Torremans, K., Kyne, R., Doyle, R., Güven, J.F., Walsh, J.J., 2018. Controls on Metal Distributions at the Lisheen and Silvermines Deposits : Insights into Fluid Flow Pathways in Irish-Type Zn-Pb Deposits. Econ. Geol. 113, 1455–1477. https://doi.org/10.5382/econgeo.2018.4598.
Vacherat, A., Mouthereau, F., Pik, R., Huyghe, D., Paquette, J.L., Christophoul, F., Loget, N., Tibari, B., 2017. Rift-to-collision sediment routing in the Pyrenees: a synthesis from sedimentological, geochronological and kinematic constraints. Earth-Sci. Rev. 172, 43–74. https://doi.org/10.1016/j.earscirev.2017.07.004.
Van Achterbergh, E., Ryan, C.G., Griffin, W.L., 2001. Glitter! User's manual. On-line Interact. Data Reduct. LA-ICPMS Microprobe 1–72.
Van den Eeckhout, B., 1986. A case study of an Mantled gneiss antiform, the Hospitalet Massif, Pyrenees (Andorra, France). Geol. Ultraiectina 45, 189.
Van den Eeckhout, B., Zwart, H.J., 1988. Hercynian crustal-scale extensional shear zone in the Pyrenees. Geology 16, 135–138. https://doi.org/10.1130/0091-7613(1988)016<0135:HCSESZ>2.3.CO;2.
Van Lichtervelde, M., Grand'Homme, A., de Saint-Blanquat, M., Olivier, P., Gerdes, A., Paquette, J.L., Melgarejo, J.C., Druguet, E., Alfonso, P., 2017. U-Pb geochronology on zircon and columbite-group minerals of the Cap de Creus pegmatites, NE Spain. Mineral. Petrol. 111. https://doi.org/10.1007/s00710-016-0455-1.
Vanderhaeghe, O., Laurent, O., Gardien, V., Moyen, J.-F., Gébelin, A., Chelle-Michou, C., Couzinié, S., Villaros, A., Bellanger, M., 2020. Flow of partially molten crust controlling construction, growth and collapse of the Variscan orogenic belt: the geologic record of the French Massif Central. BSGF - Earth Sci. Bull.. https://doi.org/10.1051/bsgf/2020013.
Velasco, F., Pesquera, A., Herrero, J.M., 1996. Lead isotope study of Zn-Pb ore deposits associated with the Basque-Cantabrian basin and Paleozoic basement, Northern Spain. Miner. Depos. 31, 84–92. https://doi.org/10.1007/BF00225398.
Vergés, J., Fernàndez, M., Martìnez, A., 2002. The Pyrenean orogen: Pre-, syn-, and post-collisional evolution. J. Virtual Explor. 8, 1–20. https://doi.org/10.3809/jvirtex.2002.00058.
Vilà, M., Pin, C., Enrique, P., Liesa, M., 2005. Telescoping of three distinct magmatic suites in an orogenic setting: generation of Hercynian igneous rocks of the Albera Massif (Eastern Pyrenees). Lithos 83, 97–127. https://doi.org/10.1016/j.lithos.2005.01.002.
Vilà, M., Pin, C., Liesa, M., Enrique, P., 2007. LPHT metamorphism in a late orogenic transpressional setting, Albera Massif, NE Iberia: implications for the geodynamic evolution of the Variscan Pyrenees. J. Metamorph. Geol. 25, 321–347. https://doi.org/10.1111/j.1525-1314.2007.00698.x.
Walter, B.F., Gerdes, A., Kleinhanns, I.C., Dunkl, I., von Eynatten, H., Kreissl, S., Markl, G., 2018. The connection between hydrothermal fluids, mineralization, tectonics and magmatism in a continental rift setting: fluorite Sm-Nd and hematite and carbonates U-Pb geochronology from the Rhinegraben in SW Germany. Geochim. Cosmochim. Acta 240, 11–42. https://doi.org/10.1016/J.GCA.2018.08.012.
Wilby, P.R., Page, A.A., Zalasiewicz, J.A., Milodowski, A.E., Williams, M., Evans, J.A., 2007. Syntectonic monazite in low-grade mudrocks: a potential geochronometer for cleavage formation?. J. Geol. Soc. London 164, 53–56. https://doi.org/10.1144/0016-76492006-035.
Wilkinson, J.J., Hitzman, M.W., 2015. The Irish Zn-Pb orefield: The view from 2014, in: Archibald, S.M., and Piercey, S.J., eds., Cur- rent perspectives in zinc deposits: Dublin,. Irish Assoc. Econ. Geol. pp. 17–35.
Williams, M.L., Jercinovic, M.J., Harlov, D.E., Budzyń, B., Hetherington, C.J., 2011. Resetting monazite ages during fluid-related alteration. Chem. Geol. 283, 218–225. https://doi.org/10.1016/j.chemgeo.2011.01.019.
Wing, B.A., Ferry, J.M., Harrison, T.M., 2003. Prograde destruction and formation of monazite and allanite during contact and regional metamorphism of pelites: petrology and geochronology. Contrib. to Mineral. Petrol. 145, 228–250. https://doi.org/10.1007/s00410-003-0446-1.
Wu, J.H., Li, H., Algeo, T.J., Jiang, W.C., Zhou, Z.K., 2018. Genesis of the Xianghualing Sn–Pb–Zn deposit, South China: a multi-method zircon study. Ore Geol. Rev. 102, 220–239. https://doi.org/10.1016/j.oregeorev.2018.09.005.
Zwart, H.J., 1979. The Geology of the Central Pyrenees, Leidse. Geol. Meded. 50, 1–74.
Zwart, H.J., 1963a. The Structural Evolution of the Paleozoïc of the Pyrenees. Geol. Rundschau 53, 170–205.
Zwart, H.J., 1963b. Metamorphic history of the Central Pyrenees, Part II. Valle de Aran. Leidse Geol. Meded. 28, 321–376.